HHS Public Access

Author manuscript

J Neurosci Methods. Author manuscript; available in PMC 2023 February 01.

Published in final edited form as:

J Neurosci Methods. 2023 February 01; 385: 109761. doi:10.1016/j.jneumeth.2022.109761.

A microfluidic perspective on conventional *in vitro* transcranial direct current stimulation methods

Han Lu[a,b,1], **Sebastian Shaner**[b,c,1], **Elisabeth Otte**[a,b,c], **Maria Asplund**[b,c,d,e,f,*,2], **Andreas Vlachos**[a,b,g,**,2]

[a]Department of Neuroanatomy, Institute of Anatomy and Cell Biology, Faculty of Medicine, University of Freiburg, Freiburg, Germany

[b]BrainLinks-BrainTools Center, University of Freiburg, Freiburg, Germany

[c]Department of Microsystems Engineering (IMTEK), University of Freiburg, Freiburg, Germany

[d]Division of Nursing and Medical Technology, Luleå University of Technology, Luleå, Sweden

[e]Freiburg Institute for Advanced Studies (FRIAS), University of Freiburg, Freiburg, Germany

[f]Department of Microtechnology and Nanoscience, Chalmers University of Technology, Gothenburg, Sweden

[g]Center for Basics in Neuromodulation (NeuroModulBasics), Faculty of Medicine, University of Freiburg, Freiburg, Germany

Abstract

Transcranial direct current stimulation (tDCS) is a promising non-invasive brain stimulation method to treat neurological and psychiatric diseases. However, its underlying neural mechanisms warrant further investigation. Indeed, dose–response interrelations are poorly understood. Placing explanted brain tissue, mostly from mice or rats, into a uniform direct current electric field (dcEF) is a well-established *in vitro* system to elucidate the neural mechanism of tDCS. Nevertheless, we will show that generating a defined, uniform, and constant dcEF throughout a brain slice is challenging. This article critically reviews the methods used to generate and calibrate a

*Correspondence to: Department of Microtechnology and Nanoscience, Chalmers University of Technology, SE-41296, Gothenburg, Sweden. maria.asplund@chalmers.se (M. Asplund). **Correspondence to: Department of Neuroanatomy, Institute of Anatomy and Cell Biology, Faculty of Medicine, University of Freiburg, Albertstrasse 17, 79104 Freiburg, Germany. andreas.vlachos@anat.uni-freiburg.de (A. Vlachos).

[1]joint first authorship

[2]joint senior authorship

CRediT authorship contribution statement

Han Lu: Conceptualization, Methodology, Formal analysis, Visualization, Writing – original draft, review & editing. **Sebastian Shaner:** Conceptualization, Methodology, Investigation, Formal analysis, Visualization, Writing – original draft, review & editing. **Elisabeth Otte:** Investigation, Writing – original draft, review & editing. **Maria Asplund:** Conceptualization, Supervision, Funding acquisition, Writing – review & editing. **Andreas Vlachos:** Conceptualization, Supervision, Funding acquisition, Writing – review & editing.

Declaration of competing interest

The authors declare that they have no known competing financial interests or personal relationships that could have appeared to influence the work reported in this paper.

Appendix A. Supplementary data

Supplementary material related to this article can be found online at https://doi.org/10.1016/j.jneumeth.2022.109761.

uniform dcEF. We use finite element analysis (FEA) to evaluate the widely used parallel electrode configuration and show that it may not reliably generate uniform dcEF within a brain slice inside an open interface or submerged chamber. Moreover, equivalent circuit analysis and measurements inside a testing chamber suggest that calibrating the dcEF intensity with two recording electrodes can inaccurately capture the true EF magnitude in the targeted tissue when specific criteria are not met. Finally, we outline why microfluidic chambers are an effective and calibration-free approach of generating spatiotemporally uniform dcEF for DCS *in vitro* studies, facilitating accurate and fine-scale dcEF adjustments. We are convinced that improving the precision and addressing the limitations of current experimental platforms will substantially improve the reproducibility of *in vitro* experimental results. A better mechanistic understanding of dose–response relations will ultimately facilitate more effective non-invasive stimulation therapies in patients.

Keywords

transcranial direct current stimulation; in vitro; direct current electric field; electrotaxis; finite element analysis

1. Introduction

Transcranial direct current stimulation (tDCS) is a brain stimulation modality currently used to treat patients with neuropsychiatric diseases (Fregni and Pascual-Leone, 2007; Flöel, 2014; Kuo et al., 2014; Chase et al., 2020; Wang et al., 2021; Balzan et al., 2022). It is also an emerging technology for non-invasively modulating neural functions and plasticity (Nitsche et al., 2003; Reis and Fritsch, 2011; Kim et al., 2017; Thibaut et al., 2017; Lu et al., 2019; Morya et al., 2019; Ghasemian-Shirvan et al., 2020). The notion of using electricity to treat diseases can be traced back to the ancient Egyptians, Greeks, and Romans, where Nile catfish and torpedo fish were used to relieve headaches in patients (Sarmiento et al., 2016). This idea evolved with time, and in the 18th century the invention of the direct current (DC) battery promoted the clinical application of DC, among other forms of electric stimulation (Sarmiento et al., 2016). After some years of exploration and abandonment, the tDCS framework re-emerged in modern neuroscience as weak DC applied via scalp electrodes in 1998 (Priori et al., 1998; Nitsche and Paulus, 2000).

Numerous studies have since used human participants to explore the parameter space of effective stimulation for tDCS (Brunoni et al., 2012). Animal models were also applied to elucidate its underlying neuronal mechanism (Jackson et al., 2016). Meanwhile, well before tDCS emerged, pilot animal studies examined electric field (EF) effects on neural responses both *in vivo* and *in vitro* (Terzuolo and Bullock, 1956; Creutzfeldt et al., 1962; Bindman et al., 1964; Jefferys, 1981). Since neurons communicate via electrochemical signals, any endogenous and exogenous EF would, in theory, affect neural activities and brain oscillations (Fröhlich and McCormick, 2010; Anastassiou et al., 2011; Anastassiou and Koch, 2015; Han et al., 2018; Rebollo et al., 2021). Under the respective themes of tDCS and EF stimulation, these two lines of research converged and paved the path for studying tDCS’s network, cellular, and molecular mechanisms in animal models.

To provide an overview of basic studies conducted on tDCS, we collected a total of 213 publications from PubMed that performed tDCS in non-human mammals (e.g., rats, mice, cats, guinea pigs, ferrets, and monkeys) or on their explanted brain tissue. We analyzed each subcategory's yearly publication counts between 1996 and 2021 (Fig. 1). Most (182) applied tDCS *in vivo*: either in naïve animals (75, black bars) to study the tDCS-induced molecular, physiological, and behavioral alterations, or in animal disease models (107, orange bars) for its potential therapeutic effects in alleviating the disease symptoms. Direct current electric fields (dcEFs) were applied *in vitro* to disentangle the effects of direct current stimulation (DCS) on neurons and non-neuron brain cells in 34 studies (Table 1). Unlike *in vivo* conditions, since it is difficult to replicate disease conditions *in vitro*, only two *in vitro* disease studies have been performed. One induced a seizure-like status (Chang et al., 2015) in mouse acute brain slices. The other created a Parkinson's disease model using human neural cells (Ross et al., 2020) to study the impacts of DC stimulation on disease mechanisms. Altogether, these studies support the notion that tDCS influences brain functions and animal behaviors by directly impacting neurons (the focus of most studies) or by using glial cells (Monai et al., 2016; Monai and Hirase, 2018; Gellner et al., 2021) and the blood–brain barrier (Shin et al., 2020) as effectors. *In vitro* experiments using explanted brain tissue are essential complements to *in vivo* experiments since they allow for better EF parameter control and target-cell accessibility with various recording and imaging techniques without additional experimental manipulation such as anesthesia or surgery (i.e., a few minutes to a few hours or days before stimulation). However, *in vitro* assays also come with disadvantages and technical challenges that will be outlined in detail in this review. In particular, we will stress the importance of analyzing the setups from an electrochemical perspective for precisely controlled and biocompatible EF administration to cells. Since the term DCS could refer to the stimulation applied to either the brain or body, we used (t)DCS in this manuscript to address *in vitro* studies with brain tissue, where the skull is already removed.

2. *In vitro* models and devices used for (t)DCS

Most *in vitro* (t)DCS studies focus on acute brain slices as an experimental platform, with a few exceptions that used dissociated cells or organotypic tissue cultures (Table 1). Specifically, acute brain slices are prepared from freshly dissected animal brains and are used immediately after preparation and transient activation (Lein et al., 2011). Depending on the animal source's age, they can remain active from several hours to several days. In contrast, organotypic slices are prepared from embryos or pups a few days post-birth and cultivated on meshes or filters to maintain an air–liquid interface within an incubator (Humpel, 2015). They are typically studied after reaching a steady state 2–3 weeks after preparation and can be readily assessed for several weeks afterward (Willems et al., 2016). While organotypic tissue cultures survive longer than acute brain slices, making them attractive as models, their preparation and cultivation are more demanding in terms of infrastructure. We could for now only identify a single study using organotypic slices (from the spinal cord) to assess long-term dcEF stimulation effects (Meng et al., 2012). Dissociated cell cultures prepared from cell lines or primary cultures (Dichter and Pollard, 2006) are also common models in (t)DCS studies (Pelletier et al., 2015; Latchoumane et

al., 2018; Ross et al., 2020; Gellner et al., 2021). However, it should be noted that in these preparations the cytoand fiber-architecture is not comparable to the *in vivo* environment.

Studying brain tissue or cells outside their innate circulatory and immune system poses several practical challenges, such as maintaining the perfusion needed to keep the explanted brain tissue viable *in vitro*. As reviewed in Huang et al. (2012), neuroscientists can house brain slices for some hours or days in a relatively standardized chamber, where carbogen-saturated artificial cerebrospinal fluid (aCSF) or culture medium flows below or over the brain tissue. Depending on the liquid–atmosphere arrangement within the chambers, they can be categorized as being either interface or submerged chambers (Fig. 2 in Huang et al. (2012)). In interface chambers, brain slices usually rest on a supported mesh or filter with their bottom surface in contact with the bath solution (aCSF or culture medium) for nutrient-waste exchange and their top surface exposed to the atmosphere. In submerged chambers, also called superfusion chambers, brain slices are entirely submerged in a solution bath and resting on a supporting surface. Both types are commonly used with acute slices or organotypic slices, while dissociated cell cultures are typically cultivated in submerged settings.

Further complexity is added when the culture chamber is integrated into electrophysiological or live-cell imaging setups that provide stimulation response readouts. From this perspective, an open chamber is beneficial as this facilitates access to the cells with recording electrodes and live-cell imaging objectives. For example, interface chambers can host local field potential (LFP) recordings and imaging with dry objectives, while submerged chambers permit whole-cell patch-clamp recordings and imaging with immersed objectives. We plotted a literature bubble map (Ma, 2021) to summarize the methodological features of prior (t)DCS studies (Fig. 2). Each dot represents an *in vitro* research article published in the corresponding year (*x*-axis). The number of studies using submerged chambers (on a light yellow background) or interface chambers (on a dark yellow background) are similar. Chronologically, the submerged chamber was first used in Jefferys' EF study (Jefferys, 1981), while the interface chamber was used later in another EF study by Andreasen and Nedergaard (Andreasen and Nedergaard, 1996). However, the order in which these chambers were applied in modern (t)DCS studies is reversed. Bikson et al. started to use the interface chambers in 2003 (Bikson et al., 2003) and 2004 (Bikson et al., 2004), applying uniform EF to their LFP recording. Later, the submerged chamber was used by Radman and colleagues to study the impact of EF with whole-cell patch-clamp recording (Radman et al., 2009a,b). In addition to classical electrophysiological devices such as LFP and whole-cell patch-clamp recordings, multi-electrode arrays (MEAs) have been recently used in combination with submerged chambers to study (t)DCS (Chang et al., 2015; Lu et al., 2016; Sun et al., 2016, 2020). While Pelletier et al. (2015) and Gellner et al. (2021) also used a submerged approach, their chamber design and EF-generation approach were quite different from the conventional open chambers, which will be discussed in the next section.

3. Approaches used to generate uniform dcEF

Brain slices subjected to a weak uniform dcEF (0.1 to 10 mV mm^{-1}) are the overwhelmingly used modality for (t)DCS studies. Due to the complex cortical geometry

of both healthy subjects and diseased patients, the tDCS-generated EF within an individual human brain is highly heterogeneous regardless of the electrode montages (Datta et al., 2010; Suh et al., 2010, 2012; Datta et al., 2013; Dmochowski et al., 2013; Edwards et al., 2013; Vöröslakos et al., 2018). However, it is reasonable to treat the EF as *quasi-uniform* at the cellular measurement scale (Bikson et al., 2013; Jackson et al., 2016). Therefore, tDCS researchers used a parallel electrode configuration for *in vitro* studies, which were used in earlier experiments (Jefferys, 1981; Andreasen and Nedergaard, 1996) to generate a uniform EF.

This parallel electrode configuration has been used in many subsequent studies (green dots in Fig. 2), where the EF is generated with parallel silver–silver chloride (Ag/AgCl) electrode wires connected to an external constant current source (i.e., galvanostat). The electrode pair is immersed in the bath solution to generate an EF between the two electrodes (gap of 10–20 mm), where the brain slice is immobilized in between (Fig. 3a–b). Despite the popularity of the parallel electrode configuration, certain assumptions need to be satisfied in order to guarantee a reliable uniform dcEF. (i) The electrodes should be placed perfectly parallel and on the same plane as the brain slice. (ii) The chamber's bath solution, which determines the electrolyte cross-sectional area across the entire brain slice, should remain constant throughout the stimulation zone. In other words, since the EF intensity is inversely proportional to the electrolyte's width (W) and height (h) (Fig. 3, right panels, also see Leal et al., 2021), researchers should avoid fluctuating the bath solution's width and height during experiments. In the case of common submerged chambers, surface tension and the interaction between the bath solution and the chamber's material(s) may cumulatively lead to an uneven liquid distribution (i.e., variable height; $h_a \neq h_b$ in Fig. 3b), and a spatially non-uniform EF distribution where it matters most (i.e., over the brain slice). The latter assumption also explains why submerged chambers used in previous studies, which had a larger electrolyte cross-sectional area than interface chambers, reported having to use a stronger input current to achieve comparable EF strength (Radman et al., 2009b). (iii) Based on the same rationale as the second assumption, the bath solution volume should also remain constant throughout the experiment in order to keep the uniform EF strength temporally steady, with laminar medium exchange compensating for any bath solution evaporation. Unfortunately, all of these assumptions have not been explicitly addressed in the method descriptions of any published study.

Aside from parallel electrodes, there are variants and alternative methods for generating dcEFs *in vitro*. For example, Fritsch et al. (2010) used commercially available conductive rubber tDCS electrodes in a non-parallel configuration (Fig. 2, white dot) and reported a non-uniform EF. Electrotaxis experiments inspired some recent cell culture studies to use microfluidic chambers for uniform dcEF generation (Pelletier et al., 2015; Gellner et al., 2021) (Fig. 2, red dots). These microfluidic chambers use the same submerged approach to organize the biological matter with gas and fluid exchange akin to conventional open chambers. However, they possess a much smaller compartment for the biological matter to be stimulated (i.e., at least one of the stimulation zone's three dimensions is less than 1 mm, thus in the microfluidic regime). Cells are seeded on a rectangular microchannel's floor (i.e., substrate) and submerged in the bath solution (Fig. 1 in Pelletier et al. (2015)). The

anode and cathode are typically not placed in the same microchannel as the cells, but instead immersed in two distinct reservoirs. The electrolyte-filled reservoirs are either directly connected to the microchannel (Fig. 2 in Gellner et al. (2021)) or indirectly connected via salt bridges typically based on saline-infused agar (Fig. 1 in Pelletier et al. (2015)). The geometry-defined stimulation zone has two purposes. First, the large difference in cross-sectional area between the reservoirs and the microchannel (i.e., large resistance difference) causes the voltage drop mostly to occur within the microchannel, thus producing a uniform EF across the entirety of the microchannel since the EF lines are funneled through the narrower opening (Asano et al., 2020). Second, the microchannel's constant cross-sectional area along its length allows for easy calculation of the generated EF strength (Pelletier et al., 2015; Leal et al., 2021), with the EF being directly proportional to the input current (i_s) and inversely proportional to the channel cross-sectional area (A) and the electrolyte conductivity (σ) (Schopf et al., 2016):

$$E = \frac{i_s}{A \cdot \sigma}, \tag{1}$$

where the electrolyte conductivity (σ) is the reciprocal of electrolyte resistivity ($\rho = \frac{1}{\sigma}$). This method to generate a uniform and calibration-free EF will be discussed in more detail in the microfluidic chamber design section.

4. Approaches used to measure and calibrate dcEF strength

When working with open chambers, a common approach is to calibrate the EF intensity via the recording electrodes of the electrophysiological setups, where the online and offline stimulation effects (the stimulation's immediate- and after-effects, respectively, when the stimulation in on and off) are recorded. Fig. 4a shows the calibration process in a submerged chamber. The constant stimulation current (i_s) that is regulated by the stimulation voltage (V_s) will flow over the circuit comprising of two electrode interfaces and the electrolyte. Two additional recording electrodes are positioned along the EF and at a defined inter-electrode distance (Δd_r). The recorded voltage difference (ΔV_r) approximates the EF intensity by $E \approx \frac{\Delta V_r}{\Delta d_r}$.

An often overlooked shortcoming of the described EF calibration procedure is that it neglects the voltage drop occurring at each recording electrode interface. Therefore, the recorded EF strength will be lower than the actual EF generated by the stimulation electrodes. We outline an equivalent circuit of the setup illustrating the underlying reason in Fig. 4b. In theory, all components within the system have resistive and capacitive components, including the recording electrodes. Since we focus on DC, the electrode's resistive behaviors will dominate, which can be approximated with a resistor (Merrill et al., 2005; Boehler et al., 2020; Das et al., 2020). This system, including brain tissue, electrolyte, two recording electrodes, and two stimulation electrodes, is equivalent to a voltage divider with five resistances: the equivalent resistance of the electrolyte-soaked brain slice between the two recording electrodes (R_{bs}), the equivalent resistances at either side of the recording circuit (i.e., the interface at each stimulating electrode plus the additional

resistance of the brain slice between the stimulating and recording electrodes (R_{bs1} and R_{bs2}), and the recording electrode interfaces (R_{e1}, R_{e2}). Ideally, the voltmeter's internal resistance is infinitely large, minimizing current extraction from the system and into the recording electrodes. Under such ideal conditions, the recorded voltage (ΔV_r) equals the voltage drop (V_{bs}) across the tissue–electrolyte mixture (R_{bs}), and $E = \frac{\Delta V_{bs}}{\Delta d_r} = \frac{\Delta V_r}{\Delta d_r}$, just as intended. However, the voltmeter's internal resistance is not infinite and therefore does not prevent the current flow (i_r) through the recording electrodes. Due to the current flow (i_r) in the measuring circuit, the recorded voltage (ΔV_r) equals the difference between V_{bs} and the voltage drop across two electrodes (V_{e1} and V_{e2}). Therefore, the resistance of the two recording electrodes eventually attenuates the measurement, causing an EF intensity underestimation $\left(E = \frac{\Delta V_{bs}}{\Delta d_r} > \frac{\Delta V_r}{\Delta d_r}\right)$.

While modern electrophysiological setups use high impedance amplifiers rather than free-standing voltmeters to minimize recording bias, the input impedances are high relative to the low electrode impedance in the high-frequency regime, as is the case of conventional spike recordings. However, for low frequencies, especially in the extreme DC signal case, the electrode impedance increases several orders of magnitude, which is a game changer for these measurements (Boehler et al., 2020). Hence, what may be considered sufficiently high input impedance for a spike recording, may be insufficient for DC regime measurements. Consequently, it is important to consider this when using electrodes to calibrate the EF and to be transparent about these aspects (i.e., electrode and input amplifier impedance in the DC regime) when reporting EF values. A voltmeter with relatively high input resistance and recording electrodes with comparably low DC resistance should be used to prevent substantial error in real versus measured EF values. The appropriate working range relationship between these two values will be discussed in the last section and is summarized in Table 2.

This scenario specifies only the condition measuring EF intensity with a brain slice inside the chamber. However, in (t)DCS studies it is often not clearly stated whether the EF intensity was calibrated with or without the brain slice. This ambiguity adds further complexity to the problem. Brain tissue is typically less conductive than the bath solution, meaning adding the brain slice changes the R_{bs} value in the equivalent circuit. Calibrating the EF intensity first and subsequently positioning the brain slice will lead to a different EF intensity within the brain tissue than expected based on the calibrated value. Electrophysiological setups use a three-electrode configuration, with two independent recording electrodes and one electrophysiological reference electrode, to measure the EF. The voltage drop over the recording electrodes remains critical. The voltage difference between the two recording electrodes is not the direct readout V_r in Fig. 4b. Instead, it is estimated by subtracting the two recorded voltages ($V_{r\_diff} = V_{r\_e1} - V_{r\_e2}$, with $V_{r\_e1} = V_{e1} - V_{ref}$ and $V_{r\_e2} = V_{e2} - V_{ref}$, respectively). Therefore, the voltage drop over the reference electrode is negated. That is, $V_r = V_{r\_diff}$, only when the reference electrode's internal resistance is identical for both recordings. Otherwise, using a three-electrode setup might further corrupt the EF estimation. Finally, when using multiple independent

electronic systems interacting over the same electrolyte, it is important to ensure that their ground connections are physically decoupled. When this is not the case, unexpected current pathways may arise, generating confusing measurements that can be challenging to troubleshoot.

In summary, the calibration method with two recording electrodes has both advantages and disadvantages. While the recording electrodes must extract sufficient energy to yield a measurement, too much energy could potentially influence the actual EF strength value. This method also assumes that the two recording electrodes are perfectly separated by a known distance (Δd_r) on a repeatable basis. The variant that uses MEAs to calibrate EF intensity follows the same principle and shares the same risks (Chang et al., 2015; Lu et al., 2016; Sun et al., 2020). While MEAs provide electrodes at well-defined electrode spacing, they may feature tiny electrodes with massive impedance in the low-frequency range, rendering them unfit for accurate dcEF monitoring. In the following sections, we will suggest how to mitigate these liabilities by emphasizing the importance of electrode material and system choice and by establishing a calibration-free design without recording electrodes.

5. FEA-based analysis of the dcEF distribution within *in vitro* devices

The potential limitations of the above calibration method, compounded with possible dynamic fluidic levels above the brain slice, raise the question of how to estimate the EF intensity precisely and whether the parallel stimulation electrodes achieve the desired EF distribution in different chamber designs. Finite element analysis (FEA) and brain imaging are frequently used in human tDCS experiments to estimate the induced EF within individual brains (Datta et al., 2010; Suh et al., 2010, 2012; Datta et al., 2013; Dmochowski et al., 2013; Edwards et al., 2013). The same principles can be used to estimate the EF distribution within the brain slices and the surrounding ionically conductive bath solution (e.g., aCSF). In order to discuss the extreme tissue–fluid interface case, we modeled the brain slice as organotypic tissue on a polytetrafluoroethylene membrane (i.e., PTFE or Teflon). We used a 3 × 3 grid of 10 μm diameter pores directly under the brain slice's center, where the tissue could grow into rather than merely resting on the membrane as in the case of an acute slice. To compare the EF distribution for different chamber designs, we modeled the same electrode–electrolyte interface area for all cases (Fig. 5a–b). The three chamber types were all modeled as rectangular in shape, except for the conventional submerged case where a surface energy-driven electrolyte meniscus above the tissue is open to the atmosphere to allow for preemptive EF probe calibration (Huang et al., 2012). Fluidic compartments dimensions and electrode sizes were extracted from prior studies (Mebane and Maier, 2010; Nishi et al., 2012; Miceli et al., 2017; Pargar et al., 2018; Asan et al., 2019) and summarized in Table 3, together with other critical input parameters.

FEA simulations confirm that for the same input current and electrode–electrolyte interface area, the induced EF is relatively weak and inhomogeneous for the conventional interface chamber (Fig. 5d,g,j), but homogeneous and 2–3 orders of magnitude stronger across the bulk of the brain tissue for both submerged chamber designs: conventional (Fig. 5e,h,k) and microfluidic chamber (Fig. 5f,i,l). The EF distribution shows greater distortion in tissue close to the membrane pores than in other locations in the interface design (Fig. 5d). This

finding suggests that these ionically conductive channels are crucial in how current and EF permeate the tissue and cause localized areas with relatively higher EF magnitudes. In this model, we simplified the membrane's pore density as a 3 × 3 grid of tissue-filled micro-pores. Higher pore density or increased pore size in actual experiments may improve the EF distribution in the tissue close to the membrane. However, the EF strength discrepancy between the bottom side close to the membrane and the top side facing the atmosphere cannot be avoided. Therefore, the effects of the membrane pores are less pronounced in the two submerged designs when the brain slice is fully submersed in the conductive electrolyte. Indeed, the EF distribution is homogeneous across the brain slice, except for the edges where the tissue model's sharp corners result in higher EF strength due to the FEA model's edge-effects. This 3D modeling artifact is not truly representative of the real-world scenario since acute or cultured brain slices will not have sharp 90° edges due to their elastic mechanical properties. Thinner tissue may be realized at the tissue boundaries in cultured brain slices due to neuron decay or migration. Depending on the tissue boundary viability, this tissue rim might also cause net positive or negative current edge-effects. However, the regions of interest are typically closer to the center of the brain slice, where the controlling of EF uniformity is more important. A closer look at the simulations shows the percentage EF intensity difference from the top edge to the tissue center is ~ 50% for the conventional submerged case with meniscus and ~ 20% for the microfluidic chamber design (Fig. 5e,f). This finding suggests that the variable height above the slice greatly affects providing a constant and uniform EF throughout the tissue. We will discuss the electrolyte height's influence in detail in the microfluidic chamber design section. Furthermore, the impact of the fluid–gas arrangement around the brain slice in both interface and submerged variations emphasizes the above point regarding calibration in the absence/presence of the slice. Placing the brain slice in the interface configuration would significantly reduce the current and EF that reaches the bulk tissue. Additionally, the ability to deliver a stronger and more uniform EF for the same input current allows for the microfluidic chamber to require less input current to provide the desired EF, thus putting less stress on the stimulation electrodes and allowing for longer stimulation periods.

6. Electrode material and arrangement effects

Electrode materials can be generally categorized as polarizable or non-polarizable, which in the stimulation context refers to the mechanisms by which they pass the charge to the surrounding electrolyte. An ideal polarizable electrode only interacts with the electrolyte via capacitive coupling, over the so-called Helmholtz double-layer (HDL). However, a non-polarizable electrode cannot build up excess charge at the electrode/electrolyte interface, and every voltage applied to the electrode immediately causes a current flow. Therefore, the electronic charge is converted into an ionic charge, with faradaic reactions at the electrode surface responsible for charge transfer.

Most electrode materials, including noble metals, are located somewhere on the spectrum between being polarizable and non-polarizable. That means, they have mixed charge injection involving both capacitive and faradaic current injection. In simple terms, the electrode can be considered connected to the electrolyte via a capacitor (i.e., HDL) in parallel with a resistor (i.e., faradaic contribution). For example, platinum can inject charge

both via the HDL and by various surface reactions involving oxygen and hydrogen within the electrolyte. Which injection mechanism dominates the injected charge depends on the electrode material, electrolyte, applied voltage, frequency, and the stimulation's current density and pulse width (Cogan, 2008; Boehler et al., 2020). Importantly, only the faradaic charge injection mechanism is relevant in the specific DC case. This is why typical neurostimulation materials, such as platinum, are usually exchanged for variants with a well-defined ion exchange chemistry, such as Ag plated with AgCl. A voltage applied between the Ag/AgCl electrodes will result in a proportional AgCl dissolution to its ions Ag^+ and Cl^- for the anode and cathode, respectively. Therefore, DC stimulation changes the electrodes' chemical composition and surroundings. Consequently, special attention should be given to the reaction products' biocompatibility when stimulation electrodes are placed in the same chamber as the tissue. For example, using Ag/AgCl electrodes releases toxic Ag^+ ions into the electrolyte via the anode (Stensaas and Stensaas, 2004; Schopf et al., 2016).

Joule heating and electrolysis are also potential threats to cell viability (Morton et al., 1994; Boehler et al., 2020). In this case, constant perfusion of fresh bath solution provides a quick fix, but this also induces a concurrent ionic flow during stimulation. Furthermore, perfusion causes variance in the electrolyte cross-sectional area in the case of conventional submerged devices. When compared to a large stimulation volume, the reduced stimulation zone that houses the tissue (i.e., microchannel) further reduces DC electrode Joule heating by requiring less input current from the stimulation electrodes for the same output EF strength. Separating the stimulation chamber and the electrode-containing reservoirs in a multi-chamber design also helps, especially when salt bridges are used as attenuation barriers for toxic ion diffusion and Joule heating dissipation. Such barriers prevent (or delay) metal ions from leeching into the microchannel and buffer the acidic and basic pH swings at the anode and cathode due to oxidation and reduction, respectively. Recently it has been highlighted that using highly porous materials such as sputtered iridium oxide films or conducting polymer-based electrodes (e.g., poly(3,4-ethylenedioxythiophene) polystyrene sulfonate - PEDOT:PSS) offers a functional alternative. It is possible to preload these porous electrodes with ions from the electrolyte, preventing products of unwanted reactions such as corrosion and enabling biocompatible DC ionic charge transfer (Boehler et al., 2020; Leal et al., 2021; Bianchi et al., 2022).

Different criteria must be considered when selecting the recording electrode material for EF calibration. The recording electrode resistance (R_{e1} and R_{e2}) depends on the material and the contact resistance (Fig. 4). The larger the contact area between the electrode and electrolyte, the lower the contact resistance (Hung et al., 2007). Another factor influencing ΔV_r is the electrode potential forming at the electrode and electrolyte interface (Merrill et al., 2005). Maintaining a constant contact area between the electrode and electrolyte is critical for maintaining a constant electrode resistance, which ensures measurement reproducibility across experiments. Any repositioning or exchange of individual electrodes, which is inevitable in practice, adds another level of uncertainty to the EF calibration. However, choosing stable and non-polarizable electrodes that are precisely fixed at known distances helps alleviate these shortcomings.

7. Microfluidic chamber design: insights from dcEF electrotaxis devices

Unlike conventional open chambers, where the brain slice is placed in a large bath solution volume, some studies used a microfluidic chamber design that divides the bath solution volume across three compartments: two reservoirs connected by a narrow rectangular microchannel. This chamber design was originally used in electrotaxis experiments, also called galvanotaxis. Electrotaxis was first described in lower organisms such as ciliate infusoria (Dale, 1901), slime mold (Anderson, 1951), brittle star (Rakshit and Brahmachary, 1974), and *Caenorhabditis elegans* (Sukul and Croll, 1978). These organisms aligned their orientation or migration direction to the EF when DC was applied. The electrotaxis concept was later applied to study embryonic cells motility (Nuccitelli and Erickson, 1983; Erickson and Nuccitelli, 1984), cultured corneal epithelial cells orientation (Zhao et al., 1996, 1997), and the migration of lymphocytes extracted from blood or bone marrow (Lin et al., 2008). In these studies (summarized in Supplementary Table 1), cells were usually seeded on a transparent substrate and immersed in the culture medium inside a narrow stimulation microchannel. Strong dcEFs at tens to hundreds of mV mm^{-1} were applied to various cell types for hours or even days to induce cell migration or morphological changes (Zhao et al., 2006; Song et al., 2007). Described as early as 1983 by Nuccitelli and Erickson (1983), the rectangular shape of the microchannel was commonplace, together with the two-reservoir design and agar bridges. Some studies used a lid to prevent evaporation and maintain the microchannel's constant cross-sectional area, while others did not. These devices were placed inside an incubator or an incubator-like chamber integrated into the live-cell microscope to maintain temperature and carbon dioxide concentration during imaging.

As discussed earlier, the microchannel experiences the dominating voltage drop within the complete system, causing a uniform EF across the entirety of the microchannel. Consequently, the submerged electrodes no longer need to be parallel to produce the uniform EF in the stimulation zone (Leal et al., 2021) (Supplementary Figure 1). The physical lid that defines the microchannel and forces the electrolyte into a rectangular format is essential for maintaining a spatiotemporally constant EF in and around the targeted brain slice. Another advantage of maintaining such a rectangular-shaped microchannel is that it allows for the generated EF to be calculated. For example, a given electrolyte with known volume resistivity (ρ) inside a given microchannel with known length (l), width (w), and height (h), the resistance of this channel is $R_{\text{channel}} = \frac{\rho \cdot l}{w \cdot h}$. The potential drop across the microchannel at any given input current intensity is readily calculated by Ohm's law ($V_{\text{channel}} = i_s \cdot R_{\text{channel}}$), as is the EF intensity (by expanding $E = \frac{V_{\text{channel}}}{l}$, we eventually get Eq. (1)). Therefore, this approach does not require calibration, since the EF intensity is precisely controlled by the current, given that the electrolyte conductivity and microchannel dimensions remain constant. Previous work has shown that changes in conductivity are negligible, as long as larger fluctuations in temperature are avoided and evaporation is limited (Schopf et al., 2016). Besides, the Debye length of a solution with a physiological salt environment (i.e., 1× or 10mM phosphate-buffered saline, PBS) at the microchannel wall boundaries is only ~ 0.8 nm (Lin et al., 2009), much smaller than the height and width of the microchannel (hundreds of μm-scale) housing the tissue. When the DC source

is turned on, the current is constantly flowing within the bulk solution. Therefore, charge accumulation at these borders is negligible compared to the charge delivered through the ionic flow within the solution. Furthermore, the microchannel's reduced dimensions permits a larger bandwidth for researchers to test various EF strengths (up to hundreds of mV mm^{-1}) using lower current, reducing both the voltage drop over the electrode interfaces and the electrochemical side-effects.

8. Investigation of the conventional dcEF strength calibration approach

In order to show the importance of the recording electrode material, configuration, and the digital measuring equipment choice, we fabricated a microfluidic chamber and performed recording trials to validate all of these points (Fig. 6, fabrication procedure is detailed in Supplementary Materials). This microfluidic chamber design has five metal recording electrodes built into the lid of the microchannel, and these recording electrodes were placed in a row at defined spacing during laser fabrication (Fig. 6a–d). DC stimulation was applied via large Ag/AgCl disk electrodes (ϕ = 12 mm, Science Products, E-204) in a charge-balanced manner (±1 mA for 2 min each) in two reservoirs (Fig. 6d). We performed systematic recordings by choosing any recording electrode pair and connecting them as the recording anode (red) and cathode (black) to a 6.5-digit precision multimeter (Agilent 34410 A) (Fig. 6d–e). The EF intensity estimation relied on the definition of recording electrode gap (Δd_r) since the recorded potential was to be divided by this number $\left(E = \frac{\Delta V_r}{\Delta d_r}\right)$. Here, we specified three gap distances: near edge to near edge (n2n), center to center (c2c), or far edge to far edge (f2f) for each pair of recording electrodes (Fig. 6f). The stimulation protocol is shown in Fig. 6g.

Our recordings confirmed the recording electrode material's influential role. The recorded potential was stable over time when using Ag/AgCl recording electrodes, but time-varying when using polarizable Ag electrodes (Fig. 6h). This finding correlated with the electrochemical impedance spectroscopy output at low frequencies (Fig. 6b), with the potential recording varying, because the Ag electrode was not in a stable non-polarizable state. Additionally, the choice of electrode pairs (i.e., distance) and their configuration relative to the stimulation electrode's location changed only the readout's sign and voltage difference magnitude (two configurations are shown in Fig. 6h). What matters is an improper definition of the recording gap. The relative difference between the expected EF intensity (i.e., the function of microchannel cross-sectional area, electrolyte conductivity, and input current) and the estimated EF intensity (i.e., dividing the measured voltage difference by corresponding gap distance) is illustrated and summarized in Fig. 6f and i, respectively. Different electrode combination gaps (from d to $4d$) were systematically examined. We found that underestimating the gap distance definition (n2n) led to a large calculation error that overestimated EF intensity (Fig. 6i, yellow bars). The calculation error varied as a function of the measured gap. However, overestimating the gap distance (f2f) led to EF underestimation (Fig. 6i, magenta bars) because the stimulation current travels up the recording electrode edge that is closest to the current source, then travels through the voltmeter (i.e., digital multimeter) and back down into the other recording electrode's leading edge, also closest to the current source (Fig. 6d, red lines). Therefore, an effective

gap distance definition is center to center, leading to consistent EF magnitudes regardless of the electrode combination gap (Fig. 6i, green bars).

Nevertheless, the estimated EF intensity by the c2c gap distance consistently showed an average underestimation of ~ 1.58%. Voltmeter input DC resistance and recording electrode DC resistances help explain this slight bias. The tissue section that is measured (in this case it is only the electrolyte-filled microchannel) has the recording electrodes connected in series and the voltmeter in parallel (Fig. 4). Thus, it would be ideal to have an infinitely high impedance for the voltmeter and an infinitely low impedance for the recording electrodes. Albeit, for the latter, it should be equal to or greater than the resistance of the tissue/channel (Table 2). In this setup, given the PBS electrolyte's conductivity (1.54 S m^{-1}), the microchannel cross-sectional area (4.391 mm^2) and the input current (1 mA), the expected voltage drop across a 5.0 mm distance (the same as adjacent recording electrodes) is 739.4 mV. However, the Ag/AgCl wire recording electrodes resistances are in the range of 65–75 kΩ (Fig. 6b), while the voltmeter input resistance is at 10 MΩ. Substituting these values into the equivalent circuit gives an anticipated percentage difference between the expected voltage (e.g., 739.4 mV) and the theoretically measured voltage (e.g., 729.2 mV) of ≈ −1.39%, close to what was found experimentally (−1.58%). While this error might be considered small for stimulation protocols, the presented measurements were obtained under ideal conditions. Measurements under non-ideal conditions, as described earlier, can result in a non-negligible increase in the error. When measuring and calibrating their EF with two electrodes in the setup, these results highlight the importance of recording electrode material, recording gap definition, gap resolution, and the impedances of the recording electrodes and the voltmeter relative to the electrolyte/tissue conductivity and channel cross-section.

Moreover, we can divide the calibration bias into two individual errors based on Ohm's law. The first error, $err_1 = \frac{R_{bs}}{R_{bs} + R_{e1} + R_{e2} + R_{V_r}}$, is caused by the measurement setup extracting too much energy from the stimulation experiment. This error results in a reduction of EF in the stimulation chamber, due to the presence of the recording equipment. The second error, $err_2 = \frac{R_{e1} + R_{e2}}{(R_{e1} + R_{e2})R_{V_r}}$, is caused by the voltage drop across recording electrodes. The more the voltage drops over the recording electrodes instead of the voltmeter, the higher the err_2. In cases where a microfluidic chamber with a rectangular microchannel is not applicable and the two-electrode calibration method has to be used, a general guideline is to have the ratio of the voltmeter input DC resistance to the sum of recording electrode DC resistances be ≥ 100. However, even when all these guidelines cannot be met, the EF can still be accurately measured when the three resistance values are known and the error can be calculated and compensated. We estimated the calibration bias in different conditions and the results are summarized in Table 2.

9. Discussions and conclusions

Non-invasive electrical stimulation paradigms have exciting therapy possibilities and can possibly offer alleviation for several serious conditions where classical pharmacological

treatments have insufficient efficacy. Electrical interventions have several advantages over pharmacological means. In particular, as the stimulation action is localized instead of systemic, it can be switched on/off instantly and does not rely on complex metabolism for its action. Despite the long historical track-record of using electrical stimulation in clinics, the understanding of tDCS mechanism remains in its infancy, to some extent. While the induced EF within individual human brains by external tDCS is non-uniform and highly subject-specific, *in vitro* systems with brain slices have enabled the dissection of individual factors later shown to be critical for EF effects on neural activity and plasticity, such as EF intensity (Bikson et al., 2004), neural somato-dendritic axis orientation inside EF (Radman et al., 2009b), axonal projection orientations (Rahman et al., 2013), and synaptic activity levels (Fritsch et al., 2010; Kronberg et al., 2020), etc. The underlying motivation for using an *in vitro* system to understand the neural mechanism of tDCS is the *quasi-uniform* assumption explicitly proposed by Bikson et al. (2013). Following this proposal, conventional submerged and interface chambers with parallel electrodes became the foundation for generating quasi-uniform dcEF. Researchers used elaborate experimental designs to elucidate the key EF-mediated neural polarization and activation mechanisms. However, this review highlights two major limitations to these studies. First, their methods to generate uniform EF within the brain slice do not reliably form a uniform EF. Second, EF intensity approximated by two electrodes systematically underestimates actual EF intensity. Therefore, the dose-dependency previously observed might not all be quantitatively accurate. Forming a uniform dcEF within a microchannel and two reservoirs frees the device from the prerequisites of parallel electrode stimulation and using calibration recording electrodes. It also minimizes the potential of DC stimulation-induced pH swings by having large buffered media reservoirs with the added benefit of a fluidic resistor to slow down the diffusion of any electrochemical faradaic by-products. However, we still acknowledge that the dose-dependency is qualitatively accurate. With this review's more tailored design, we should expect a similar dose-dependency but with more confidence in the exact EF intensities and distribution. Therefore, the new microfluidic chamber design allows us to replicate and reexamine the cornerstone-like conclusions based on the conventional designs and to justify them from a different perspective.

Indeed, the tDCS field has been aware of the limitations of the conventional experimental approaches, and pioneering research is seeking alternatives. Radman et al. reported that the submerged chamber requires a stronger input current to achieve comparable EF strength as the interface chamber (Radman et al., 2009b). An MEA-based study measured activity dynamics within a brain slice altered by DC stimulation, finding a substantially different EF intensity inside aCSF and near the electrode surface (Sun et al., 2020). These findings suggest that calibrating EF intensity is not sufficiently reliable. While some recent studies have started using microfluidic chamber designs to generate reproducible dcEF (Meng et al., 2012; Pelletier et al., 2015; Gellner et al., 2021), they have been restricted to dissociated cell cultures. Therefore, we proposed that the microfluidic chamber would be suitable for (t)DCS studies with brain slices by adding a lid to prevent EF distribution disturbances that might arise from bath solution perfusion or evaporation. Some technical challenges may still come along. For example, a solid lid will restrict accessibility of recording electrodes or immersed objectives, which are commonly required to assess the online and offline (t)DCS effects.

In addition, the long-term viability of submerged brain slices must also be considered in this setting. Here, the microfluidic chamber design should be fully customized to perform (t)DCS studies with rodent or human brain slices. For example, improving the lid design and using advanced sensors could expand the experimental possibilities. Future key advancements for (t)DCS studies may involve using non-invasive assessments, reversibly fixing the solid lid and microchannel around the slice, substituting the solid lid with alternative options such as immiscible microfluidic lids (Brewer et al., 2014; Soitu et al., 2018, 2019), or integrating advanced MEAs into the microfluidic chamber design. Moreover, combining organotypic brain slice cultures with microfluidic chamber designs will extend the experimental assessment window. Ultimately, this new chamber design will advance our mechanistic understanding of EF dose–response interrelations and improve the reproducibility of *in vitro* experiments and the translation of tDCS findings.

It should be noted that a non-uniform EF also polarizes and activates neurons. However, a uniform EF is essential for studying the interaction between EF properties and neural responses, as well as the interference between exogenous and endogenous EFs generated by neurons. In addition to tDCS, a microfluidic chamber that provides precise EF control may facilitate the investigation of the underlying mechanisms of other electric brain stimulation techniques. For example, transcranial alternating current stimulation (tACS) (Antal et al., 2008) and transcranial random noise stimulation (tRNS) (Terney et al., 2008) are also classified as non-invasive brain stimulation (NIBS) methods. While they use a scalp electrode montage and sub-threshold EF intensity similar to tDCS, both use an alternating current containing a specific or wide range of oscillation frequencies, respectively. Electroconvulsive therapy (ECT) is also used non-invasively on the brain, but its supra-threshold intensity induces seizure-like brain activity (Feldman et al., 1945a,b; Di Iorio et al., 2022). Similarly, transcranial magnetic stimulation is also believed to stimulate brain tissue by the induced electric current from a time-varying magnetic field that is originally produced by a time-varying current in the coil (Barker et al., 1985). Despite various stimulation formats and parameters, an EF, induced or not, with varied frequency and intensity is the potentially shared active factor. A device that enables researchers to reliably study the effects of dcEF on brain tissue will contribute to dissect the mechanisms of all these complex forms of stimulation and ultimately support their therapeutic applications.

In summary, the overarching goal of tDCS *in vitro* studies is to understand its molecular, cellular, and network mechanisms and to optimize the protocols used in clinical practice. Therefore, several years of exploration using conventional chambers have made substantial progress at the level of neural somata-dendritic axis direction and membrane potential depolarization. However, their intrinsic limitations have led to qualitatively correct but possibly quantitatively imprecise dose–response curves, ill-suited to inform safety guidelines for human studies. Fortunately, new microfluidic techniques have allowed us to further enhance *in vitro* studies with more precise control over the dcEF distribution and intensity. We hope that the new design, integrating the advantages of microfluidic chambers, will help to replicate major findings obtained with animal brain tissue in conventional chambers and also provide the possibility to host human tissue under examination for longer periods.

Supplementary Material

Refer to Web version on PubMed Central for supplementary material.

Acknowledgment

The authors thank Lukas Matter for the valuable comments and suggestions on the manuscript.

Supportive Information

AV & EO: National Institutes of Health, USA (NIH; 1R01NS109498) and by the Federal Ministry of Education and Research, Germany (BMBF, 01GQ1804A).

MA & SS: European Research Council (ERC; 759655; SPEEDER) under the European Union's Horizon 2020 Research and Innovation program.

MA: Freiburg Institute for Advanced Studies (FRIAS) and Brainlinks-BrainTools which are funded by the German Research Foundation, Germany (DFG; EXC 1086) and is currently funded by the Federal Ministry of Economics, Science and Arts of Baden Württemberg, Germany within the sustainability program for projects of the excellence initiative.

Data availability

Data will be made available on request.

References

Anastassiou CA, Koch C, 2015. Ephaptic coupling to endogenous electric field activity: why bother? Curr. Opin. Neurobiol 31, 95–103. [PubMed: 25265066]

Anastassiou CA, Perin R, Markram H, Koch C, 2011. Ephaptic coupling of cortical neurons. Nature Neurosci. 14 (2), 217–223. [PubMed: 21240273]

Anderson JD, 1951. Galvanotaxis of slime mold. J. General Physiol 35 (1), 1–16.

Andreasen M, Nedergaard S, 1996. Dendritic electrogenesis in rat hippocampal CA1 pyramidal neurons: functional aspects of Na^+ and Ca^{2+} currents in apical dendrites. Hippocampus 6 (1), 79–95. [PubMed: 8878746]

Antal A, Boros K, Poreisz C, Chaieb L, Terney D, Paulus W, 2008. Comparatively weak after-effects of transcranial alternating current stimulation (tACS) on cortical excitability in humans. Brain Stimul. 1 (2), 97–105. [PubMed: 20633376]

Asan AS, Gok S, Sahin M, 2019. Electrical fields induced inside the rat brain with skin, skull, and dural placements of the current injection electrode. PLOS ONE 14 (1), e0203727.

Asano N, Kawano S, et al. , 2020. Development of glass micro-electrodes for local electric field, electrical conductivity, and pH measurements. Sci. Rep 10 (1), 1–12. [PubMed: 31913322]

Balzan P, Tattersall C, Palmer R, 2022. Non-invasive brain stimulation for treating neurogenic dysarthria: A systematic review. Ann. Phys. Rehabil. Med 65 (5), 101580.

Barker AT, Jalinous R, Freeston IL, 1985. Non-invasive magnetic stimulation of human motor cortex. Lancet 325 (8437), 1106–1107.

Bianchi M, De Salvo A, Asplund M, Carli S, Di Lauro M, Schulze-Bonhage A, et al., 2022. Poly (3, 4-ethylenedioxythiophene)-based neural interfaces for recording and stimulation: Fundamental aspects and in Vivo applications. Adv. Sci e2104701, Weinheim, Baden-Wurttemberg, Germany.

Bikson M, Dmochowski J, Rahman A, 2013. The ''quasi-uniform'' assumption in animal and computational models of non-invasive electrical stimulation. Brain Stimul. 6 (4), 704. [PubMed: 23290681]

Bikson M, Hahn PJ, Fox JE, Jefferys JG, 2003. Depolarization block of neurons during maintenance of electrographic seizures. J. Neurophysiol 90 (4), 2402–2408. [PubMed: 12801897]

Bikson M, Inoue M, Akiyama H, Deans JK, Fox JE, Miyakawa H, et al. , 2004. Effects of uniform extracellular DC electric fields on excitability in rat hippocampal slices in vitro. J. Physiol 557 (1), 175–190. [PubMed: 14978199]

Bindman LJ, Lippold O, Redfearn J, 1964. The action of brief polarizing currents on the cerebral cortex of the rat (1) during current flow and (2) in the production of long-lasting after-effects. J. Physiol 172 (3), 369–382. [PubMed: 14199369]

Boehler C, Carli S, Fadiga L, Stieglitz T, Asplund M, 2020. Tutorial: guidelines for standardized performance tests for electrodes intended for neural interfaces and bioelectronics. Nat. Protoc 15, 3557–3578. [PubMed: 33077918]

Bolzoni F, Pettersson L-G, Jankowska E, 2013. Evidence for long-lasting subcortical facilitation by transcranial direct current stimulation in the cat. J. Physiol 591 (13), 3381–3399. [PubMed: 23507876]

Brewer BM, Shi M, Edd JF, Webb DJ, Li D, 2014. A microfluidic cell co-culture platform with a liquid fluorocarbon separator. Biomed. Microdev 16 (2), 311–323.

Brunoni AR, Nitsche MA, Bolognini N, Bikson M, Wagner T, Merabet L, et al. , 2012. Clinical research with transcranial direct current stimulation (tDCS): challenges and future directions. Brain Stimul. 5 (3), 175–195. [PubMed: 22037126]

Chakraborty D, Truong DQ, Bikson M, Kaphzan H, 2018. Neuromodulation of axon terminals. Cerebral Cortex 28 (8), 2786–2794. [PubMed: 28655149]

Chang W-P, Lu H-C, Shyu B-C, 2015. Treatment with direct-current stimulation against cingulate seizure-like activity induced by 4-aminopyridine and bicuculline in an in vitro mouse model. Exper. Neurol 265, 180–192. [PubMed: 25682917]

Chase HW, Boudewyn MA, Carter CS, Phillips ML, 2020. Transcranial direct current stimulation: a roadmap for research, from mechanism of action to clinical implementation. Mol. Psychiatry 25 (2), 397–407. [PubMed: 31455860]

Cogan SF, 2008. Neural stimulation and recording electrodes. Annu. Rev. Biomed. Eng 10 (1), 275–309, arXiv:10.1146/annurev.bioeng.10.061807.160518. [PubMed: 18429704]

Creutzfeldt OD, Fromm GH, Kapp H, 1962. Influence of transcortical dc currents on cortical neuronal activity. Exper. Neurol 5 (6), 436–452. [PubMed: 13882165]

Dale H, 1901. Galvanotaxis and chemotaxis of ciliate infusoria: Part I. J. Physiol 26 (5), 291. [PubMed: 16992550]

D'Andola M, Giulioni M, Dante V, Del Giudice P, Sanchez-Vives MV, 2019. Control of cortical oscillatory frequency by a closed-loop system. J. Neuroeng. Rehabil 16 (1), 1–14. [PubMed: 30606226]

D'Andola M, Weinert JF, Mattia M, Sanchez-Vives MV, 2018. Modulation of slow and fast oscillations by direct current stimulation in the cerebral cortex in vitro. BioRxiv 246819.

Das R, Moradi F, Heidari H, 2020. Biointegrated and wirelessly powered implantable brain devices: A review. IEEE Trans. Biomed. Circuits Syst 14 (2), 343–358. [PubMed: 31944987]

Datta A, Bikson M, Fregni F, 2010. Transcranial direct current stimulation in patients with skull defects and skull plates: high-resolution computational FEM study of factors altering cortical current flow. NeuroImage 52 (4), 1268–1278. [PubMed: 20435146]

Datta A, Dmochowski JP, Guleyupoglu B, Bikson M, Fregni F, 2013. Cranial electrotherapy stimulation and transcranial pulsed current stimulation: a computer based high-resolution modeling study. NeuroImage 65, 280–287. [PubMed: 23041337]

Di Iorio R, Rossi S, Rossini PM, 2022. One century of healing currents into the brain from the scalp: From electroconvulsive therapy to repetitive transcranial magnetic stimulation for neuropsychiatric disorders. Clin. Neurophysiol 133, 145–151. [PubMed: 34864511]

Dichter MA, Pollard J, 2006. Cell culture models for studying epilepsy. In: Models of Seizures and Epilepsy. Elsevier Academic Burlington, MA, pp. 23–34.

Ding J, Hu X, Xu F, Yu H, Ye Z, Zhang S, et al. , 2021. Suppression of top-down influence decreases neuronal excitability and contrast sensitivity in the V1 cortex of cat. Sci. Rep 11 (1), 1–15. [PubMed: 33414495]

Dmochowski JP, Datta A, Huang Y, Richardson JD, Bikson M, Fridriksson J, et al. , 2013. Targeted transcranial direct current stimulation for rehabilitation after stroke. NeuroImage 75, 12–19. [PubMed: 23473936]

Edwards D, Cortes M, Datta A, Minhas P, Wassermann EM, Bikson M, 2013. Physiological and modeling evidence for focal transcranial electrical brain stimulation in humans: a basis for high-definition tDCS. NeuroImage 74, 266–275. [PubMed: 23370061]

Erickson CA, Nuccitelli R, 1984. Embryonic fibroblast motility and orientation can be influenced by physiological electric fields. J. Cell Biol 98 (1), 296–307. [PubMed: 6707093]

Esmaeilpour Z, Jackson M, Kronberg G, Zhang T, Esteller R, Hershey B, et al. , 2020. Limited sensitivity of hippocampal synaptic function or network oscillations to unmodulated kilohertz electric fields. ENeuro 7 (6).

Farahani F, Kronberg G, FallahRad M, Oviedo HV, Parra LC, 2021. Effects of direct current stimulation on synaptic plasticity in a single neuron. Brain Stimul. 14 (3), 588–597. [PubMed: 33766677]

Feldman F, Susselman S, Barrera SE, 1945a. Electroconvulsive therapy in the Prone position. J. Nervous Mental Dis 102 (5), 496–497.

Feldman F, Susselman S, Lipetz B, Barrera SE, 1945b. Electroconvulsive therapy of acute hysteria. J. Nervous Mental Dis 102 (5), 498–500.

Flöel A, 2014. TDCS-enhanced motor and cognitive function in neurological diseases. NeuroImage 85, 934–947. [PubMed: 23727025]

Fregni F, Pascual-Leone A, 2007. Technology insight: noninvasive brain stimulation in neurology—perspectives on the therapeutic potential of rTMS and tDCS. Nat. Clin. Pract. Neurol 3 (7), 383–393. [PubMed: 17611487]

Fritsch B, Reis J, Martinowich K, Schambra HM, Ji Y, Cohen LG, et al. , 2010. Direct current stimulation promotes BDNF-dependent synaptic plasticity: potential implications for motor learning. Neuron 66 (2), 198–204. [PubMed: 20434997]

Fröhlich F, McCormick DA, 2010. Endogenous electric fields may guide neocortical network activity. Neuron 67 (1), 129–143. [PubMed: 20624597]

Gellner A-K, Reis J, Fiebich BL, Fritsch B, 2021. Electrified microglia: Impact of direct current stimulation on diverse properties of the most versatile brain cell. Brain Stimul. 14 (5), 1248–1258. [PubMed: 34411753]

Ghasemian-Shirvan E, Farnad L, Mosayebi-Samani M, Verstraelen S, Meesen RL, Kuo M-F, et al. , 2020. Age-related differences of motor cortex plasticity in adults: a transcranial direct current stimulation study. Brain Stimul. 13 (6), 1588–1599. [PubMed: 32949779]

Han K-S, Guo C, Chen CH, Witter L, Osorno T, Regehr WG, 2018. Ephaptic coupling promotes synchronous firing of cerebellar purkinje cells. Neuron 100 (3), 564–578. [PubMed: 30293822]

Huang Y, Williams JC, Johnson SM, 2012. Brain slice on a chip: opportunities and challenges of applying microfluidic technology to intact tissues. Lab on A Chip 12 (12), 2103–2117. [PubMed: 22534786]

Humpel C, 2015. Organotypic brain slice cultures: A review. Neuroscience 305, 86–98. [PubMed: 26254240]

Hung A, Zhou DD, Greenberg RJ, Goldberg IB, Judy JW, 2007. Pulse-clamp technique for characterizing neural-stimulating electrodes. J. Electrochem. Soc 154.

Jackson MP, Rahman A, Lafon B, Kronberg G, Ling D, Parra LC, et al. , 2016. Animal models of transcranial direct current stimulation: methods and mechanisms. Clin. Neurophysiol 127 (11), 3425–3454. [PubMed: 27693941]

Jefferys J, 1981. Influence of electric fields on the excitability of granule cells in guinea-pig hippocampal slices. J. Physiol 319 (1), 143–152. [PubMed: 7320909]

Kabakov AY, Muller PA, Pascual-Leone A, Jensen FE, Rotenberg A, 2012. Contribution of axonal orientation to pathway-dependent modulation of excitatory transmission by direct current stimulation in isolated rat hippocampus. J. Neurophysiol 107 (7), 1881–1889. [PubMed: 22219028]

Kim MS, Koo H, Han SW, Paulus W, Nitsche MA, Kim Y-H, et al. , 2017. Repeated anodal transcranial direct current stimulation induces neural plasticity-associated gene expression in the rat cortex and hippocampus. Restor. Neurol. Neurosci 35 (2), 137–146. [PubMed: 28059801]

Krause MR, Zanos TP, Csorba BA, Pilly PK, Choe J, Phillips ME, et al. , 2017. Transcranial direct current stimulation facilitates associative learning and alters functional connectivity in the primate brain. Curr. Biol 27 (20), 3086–3096. [PubMed: 29033331]

Kronberg G, Bridi M, Abel T, Bikson M, Parra LC, 2017. Direct current stimulation modulates LTP and LTD: activity dependence and dendritic effects. Brain Stimul. 10 (1), 51–58. [PubMed: 28104085]

Kronberg G, Rahman A, Sharma M, Bikson M, Parra LC, 2020. Direct current stimulation boosts hebbian plasticity in vitro. Brain Stimul. 13 (2), 287–301. [PubMed: 31668982]

Kuo M-F, Paulus W, Nitsche MA, 2014. Therapeutic effects of non-invasive brain stimulation with direct currents (tDCS) in neuropsychiatric diseases. NeuroImage 85, 948–960. [PubMed: 23747962]

Lafon B, Rahman A, Bikson M, Parra LC, 2017. Direct current stimulation alters neuronal input/output function. Brain Stimul. 10 (1), 36–45. [PubMed: 27717601]

Latchoumane C-FV, Jackson L, Sendi MSE, Tehrani KF, Mortensen LJ, Stice SL, et al. , 2018. Chronic electrical stimulation promotes the excitability and plasticity of ESC-derived neurons following glutamate-induced inhibition in vitro. Sci. Rep 8 (1), 1–16. [PubMed: 29311619]

Leal J, Jedrusik N, Shaner S, Boehler C, Asplund M, 2021. SIROF stabilized PEDOT/PSS allows biocompatible and reversible direct current stimulation capable of driving electrotaxis in cells. Biomaterials 275, 120949.

Lein PJ, Barnhart CD, Pessah IN, 2011. Acute hippocampal slice preparation and hippocampal slice cultures. In: Vitro Neurotoxicology. Springer, pp. 115–134.

Lian J, Bikson M, Sciortino C, Stacey WC, Durand DM, 2003. Local suppression of epileptiform activity by electrical stimulation in rat hippocampus in vitro. J. Physiol 547 (2), 427–434. [PubMed: 12562909]

Lin F, Baldessari F, Gyenge CC, Sato T, Chambers RD, Santiago JG, et al. , 2008. Lymphocyte electrotaxis in vitro and in vivo. J. Immunol 181 (4), 2465–2471. [PubMed: 18684937]

Lin S-P, Pan C-Y, Tseng K-C, Lin M-C, Chen C-D, Tsai C-C, et al. , 2009. A reversible surface functionalized nanowire transistor to study protein–protein interactions. Nano Today 4 (3), 235–243.

Lu H-C, Chang W-J, Chang W-P, Shyu B-C, 2016. Direct-current stimulation and multi-electrode array recording of seizure-like activity in mice brain slice preparation. J. Vis. Exper. JoVE 112.

Lu H, Gallinaro JV, Rotter S, 2019. Network remodeling induced by transcranial brain stimulation: A computational model of tDCS-triggered cell assembly formation. Netw. Neurosci 3 (4), 924–943. [PubMed: 31637332]

Ma L, 2021. Kirsche: Connecting your references. 10.5281/zenodo.5655508, GitHub URL https://github.com/kausalflow/kirsche.

Mebane DS, Maier J, 2010. DC conductivity and dielectric properties in silver chloride, revisited. Phys. Chem. Chem. Phys 12 (10), 2478–2487. [PubMed: 20449362]

Meng X, Li W, Young F, Gao R, Chalmers L, Zhao M, et al. , 2012. Electric field-controlled directed migration of neural progenitor cells in 2D and 3D environments. J. Vis. Exper. JoVE 60.

Merrill DR, Bikson M, Jefferys JG, 2005. Electrical stimulation of excitable tissue: design of efficacious and safe protocols. J. Neurosci. Methods 141 (2), 171–198, URL https://www.sciencedirect.com/science/article/pii/S0165027004003826. [PubMed: 15661300]

Miceli S, Ness TV, Einevoll GT, Schubert D, 2017. Impedance spectrum in cortical tissue: Implications for propagation of LFP signals on the microscopic level. ENeuro 4 (1).

Monai H, Hirase H, 2018. Astrocytes as a target of transcranial direct current stimulation (tDCS) to treat depression. Neurosci. Res 126, 15–21. [PubMed: 29079367]

Monai H, Ohkura M, Tanaka M, Oe Y, Konno A, Hirai H, et al. , 2016. Calcium imaging reveals glial involvement in transcranial direct current stimulation-induced plasticity in mouse brain. Nature Commun. 7 (1), 1–10.

Morton SL, Daroux ML, Mortimer JT, 1994. The role of oxygen reduction in electrical stimulation of neural tissue. J. Electrochem. Soc 141, 122–130.

Morya E, Monte-Silva K, Bikson M, Esmaeilpour Z, Biazoli CE, Fonseca A, et al. , 2019. Beyond the target area: an integrative view of tDCS-induced motor cortex modulation in patients and athletes. J. Neuroeng. Rehabil 16 (1), 1–29. [PubMed: 30606226]

Nishi Y, Iizuka S, Faudree MC, Oyama R, 2012. Electrical conductivity enhancement of PTFE (teflon) induced by homogeneous low voltage electron beam irradiation (HLEBI). Mater. Trans 53 (5), 940–945.

Nitsche MA, Fricke K, Henschke U, Schlitterlau A, Liebetanz D, Lang N, et al. , 2003. Pharmacological modulation of cortical excitability shifts induced by transcranial direct current stimulation in humans. J. Physiol 553 (1), 293–301. [PubMed: 12949224]

Nitsche MA, Paulus W, 2000. Excitability changes induced in the human motor cortex by weak transcranial direct current stimulation. J. Physiol 527 (3), 633–639. [PubMed: 10990547]

Nuccitelli R, Erickson CA, 1983. Embryonic cell motility can be guided by physiological electric fields. Exper. Cell Res 147 (1), 195–201. [PubMed: 6617761]

Pan D, Pan H, Zhang S, Yu H, Ding J, Ye Z, et al. , 2021. Top-down influence affects the response adaptation of V1 neurons in cats. Brain Res. Bull 167, 89–98. [PubMed: 33333174]

Pargar F, Kolev H, Koleva DA, van Breugel K, 2018. Microstructure, surface chemistry and electrochemical response of Ag|AgCl sensors in alkaline media. J. Mater. Sci 53 (10), 7527–7550.

Pelletier SJ, Lagacé M, St-Amour I, Arsenault D, Cisbani G, Chabrat A, et al. , 2015. The morphological and molecular changes of brain cells exposed to direct current electric field stimulation. Int. J. Neuropsychopharmacol 18 (5).

Priori A, Berardelli A, Rona S, Accornero N, Manfredi M, 1998. Polarization of the human motor cortex through the scalp. Neuroreport 9 (10), 2257–2260. [PubMed: 9694210]

Radman T, Datta A, Ramos RL, Brumberg JC, Bikson M, 2009a. One-dimensional representation of a neuron in a uniform electric field. In: 2009 Annual International Conference of the IEEE Engineering in Medicine and Biology Society. IEEE, pp. 6481–6484.

Radman T, Parra L, Bikson M, 2006. Amplification of small electric fields by neurons; implications for spike timing. In: 2006 International Conference of the IEEE Engineering in Medicine and Biology Society. IEEE, pp. 4949–4952.

Radman T, Ramos RL, Brumberg JC, Bikson M, 2009b. Role of cortical cell type and morphology in subthreshold and suprathreshold uniform electric field stimulation in vitro. Brain Stimul. 2 (4), 215–228. [PubMed: 20161507]

Radman T, Su Y, An JH, Parra LC, Bikson M, 2007. Spike timing amplifies the effect of electric fields on neurons: implications for endogenous field effects. J. Neurosci 27 (11), 3030–3036. [PubMed: 17360926]

Rahman A, Lafon B, Parra LC, Bikson M, 2017. Direct current stimulation boosts synaptic gain and cooperativity in vitro. J. Physiol 595 (11), 3535–3547. [PubMed: 28436038]

Rahman A, Reato D, Arlotti M, Gasca F, Datta A, Parra LC, Bikson M, 2013. Cellular effects of acute direct current stimulation: somatic and synaptic terminal effects. J. Physiol 591 (10), 2563–2578. [PubMed: 23478132]

Rakshit B, Brahmachary R, 1974. Electrotaxis of the brittle star. Zeitschrift FÜR Naturforschung C 29 (9–10), 656.

Ranieri F, Podda MV, Riccardi E, Frisullo G, Dileone M, Profice P, et al. , 2012. Modulation of LTP at rat hippocampal CA3-CA1 synapses by direct current stimulation. J. Neurophysiol 107 (7), 1868–1880. [PubMed: 22236710]

Reato D, Bikson M, Parra LC, 2015. Lasting modulation of in vitro oscillatory activity with weak direct current stimulation. J. Neurophysiol 113 (5), 1334–1341. [PubMed: 25505103]

Reato D, Rahman A, Bikson M, Parra LC, 2010. Low-intensity electrical stimulation affects network dynamics by modulating population rate and spike timing. J. Neurosci 30 (45), 15067–15079. [PubMed: 21068312]

Rebollo B, Telenczuk B, Navarro-Guzman A, Destexhe A, Sanchez-Vives MV, 2021. Modulation of intercolumnar synchronization by endogenous electric fields in cerebral cortex. Sci. Adv 7 (10), eabc7772.

Reis J, Fritsch B, 2011. Modulation of motor performance and motor learning by transcranial direct current stimulation. Curr. Opin. Neurol 24 (6), 590–596. [PubMed: 21968548]

Ross A, Xing V, Wang TT, Bureau SC, Link GA, Fortin T, et al. , 2020. Alleviating toxic α-synuclein accumulation by membrane depolarization: evidence from an in vitro model of Parkinson's disease. Mol. Brain 13 (1), 1–11. [PubMed: 31900209]

Sarmiento C, San-Juan D, Prasath V, 2016. Letter to the editor: Brief history of transcranial direct current stimulation (tDCS): from electric fishes to microcontrollers. Psychol. Med 46 (15), 3259–3261. [PubMed: 27572999]

Schopf A, Boehler C, Asplund M, 2016. Analytical methods to determine electrochemical factors in electrotaxis setups and their implications for experimental design. Bioelectrochemistry 109, 41–48. [PubMed: 26775205]

Schweid L, Rushmore R, Valero-Cabre A, 2008. Cathodal transcranial direct current stimulation on posterior parietal cortex disrupts visuo-spatial processing in the contralateral visual field. Exp. Brain Res 186 (3), 409–417. [PubMed: 18196224]

Shin DW, Fan J, Luu E, Khalid W, Xia Y, Khadka N, et al. , 2020. In vivo modulation of the blood–brain barrier permeability by transcranial direct current stimulation (tDCS). Ann. Biomed. Eng 48 (4), 1256–1270. [PubMed: 31916126]

Soitu C, Feuerborn A, Deroy C, Castrejón-Pita AA, Cook PR, Walsh EJ, 2019. Raising fluid walls around living cells. Sci. Adv 5 (6), eaav8002. [PubMed: 31183401]

Soitu C, Feuerborn A, Tan AN, Walker H, Walsh PA, Castrejón-Pita A.A.a., 2018. Microfluidic chambers using fluid walls for cell biology. Proc. Natl. Acad. Sci 115 (26), E5926–E5933. [PubMed: 29895687]

Song B, Gu Y, Pu J, Reid B, Zhao Z, Zhao M, 2007. Application of direct current electric fields to cells and tissues in vitro and modulation of wound electric field in vivo. Nat. Protoc 2 (6), 1479–1489. [PubMed: 17545984]

Stensaas S, Stensaas LJ, 2004. Histopathological evaluation of materials implanted in the cerebral cortex. Acta Neuropathologica 41, 145–155.

Suh HS, Lee WH, Cho YS, Kim J-H, Kim T-S, 2010. Reduced spatial focality of electrical field in tDCS with ring electrodes due to tissue anisotropy. In: 2010 Annual International Conference of the IEEE Engineering in Medicine and Biology. IEEE, pp. 2053–2056.

Suh HS, Lee WH, Kim T-S, 2012. Influence of anisotropic conductivity in the skull and white matter on transcranial direct current stimulation via an anatomically realistic finite element head model. Phys. Med. Biol 57 (21), 6961. [PubMed: 23044667]

Sukul NC, Croll NA, 1978. Influence of potential difference and current on the electrotaxis of Caenorhaditis elegans. J. Nematol 10 (4), 314. [PubMed: 19305860]

Sun Y, Dhamne SC, Carretero-Guillén A, Salvador R, Goldenberg MC, Godlewski BR, et al. , 2020. Drug-responsive inhomogeneous cortical modulation by direct current stimulation. Ann. Neurol 88 (3), 489–502. [PubMed: 32542794]

Sun Y, Lipton JO, Boyle LM, Madsen JR, Goldenberg MC, Pascual-Leone A, et al. , 2016. Direct current stimulation induces mGluR5-dependent neocortical plasticity. Ann. Neurol 80 (2), 233–246. [PubMed: 27315032]

Terney D, Chaieb L, Moliadze V, Antal A, Paulus W, 2008. Increasing human brain excitability by transcranial high-frequency random noise stimulation. J. Neurosci 28 (52), 14147–14155. [PubMed: 19109497]

Terzuolo C, Bullock T, 1956. Measurement of imposed voltage gradient adequate to modulate neuronal firing. Proc. Natl. Acad. Sci. USA 42 (9), 687. [PubMed: 16589932]

Thibaut A, Russo C, Morales-Quezada L, Hurtado-Puerto A, Deitos A, Freedman S, Carvalho S, Fregni F, 2017. Neural signature of tDCS, tPCS and their combination: comparing the effects on neural plasticity. Neurosci. Lett 637, 207–214. [PubMed: 27765610]

Valdés-Cruz A, Villasana-Salazar B, Williams B, Martínez-Vargas D, MagdalenoMadrigal VM, Almazán-Alvarado S, Besio WG, 2019. Transcranial focal electrical stimulation via concentric ring electrodes in freely moving cats: Antiepileptogenic and postictal effects. Exper. Neurol 320, 113012.

Vasu SO, Kaphzan H, 2021. The role of sodium channels in direct current stimulation—axonal perspective. Cell Rep. 37 (2), 109832.

Vöröslakos M, Takeuchi Y, Brinyiczki K, Zombori T, Oliva A, Fernández-Ruiz A, et al. , 2018. Direct effects of transcranial electric stimulation on brain circuits in rats and humans. Nature Commun. 9 (1), 1–17. [PubMed: 29317637]

Wang S-M, Chan Y-W, Tsui Y-O, Chu F-Y, 2021. Effects of anodal cerebellar transcranial direct current stimulation on movements in patients with cerebellar?ataxias: A systematic review. Int. J. Environ. Res. Public Health 18 (20), 10690.

Willems LM, Zahn N, Ferreirós N, Scholich K, Maggio N, Deller T, et al. , 2016. Sphingosine-1-phosphate receptor inhibition prevents denervation-induced dendritic atrophy. Acta Neuropathol. Commun 4 (1), 1–12. [PubMed: 26727948]

Zhao M, Agius-Fernandez A, Forrester JV, McCaig CD, 1996. Orientation and directed migration of cultured corneal epithelial cells in small electric fields are serum dependent. J. Cell Sci 109 (6), 1405–1414. [PubMed: 8799828]

Zhao X, Ding J, Pan H, Zhang S, Pan D, Yu H, et al. , 2020. Anodal and cathodal tDCS modulate neural activity and selectively affect GABA and glutamate syntheses in the visual cortex of cats. J. Physiol 598 (17), 3727–3745. [PubMed: 32506434]

Zhao M, McCaig CD, Agius-Fernandez A, Forrester JV, Araki-Sasaki K, 1997. Human corneal epithelial cells reorient and migrate cathodally in a small applied electric field. Curr. Eye Res 16 (10), 973–984. [PubMed: 9330848]

Zhao M, Song B, Pu J, Wada T, Reid B, Tai G, et al. , 2006. Electrical signals control wound healing through phosphatidylinositol-3-OH kinase-γ and PTEN. Nature 442 (7101), 457–460. [PubMed: 16871217]

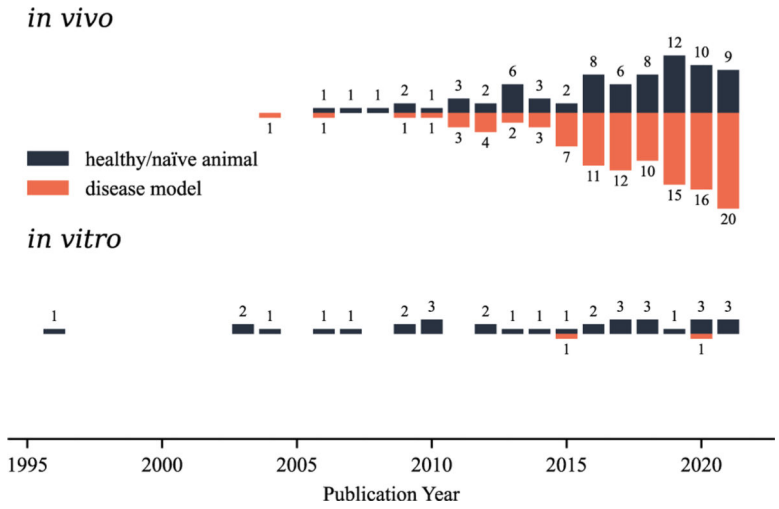

Fig. 1.

Overview of tDCS animal studies published between 1996 and 2021. We collected 270 papers from PubMed with the keywords combination ((**rat** OR **mouse**) AND (**transcranial direct current stimulation**)) in all fields. 69 papers were excluded as they are either non-English, comments and reviews, computational models, hardware and software, human studies, or contain stimulation methods that do not use DC. Two additional papers were included based on the citation history of all the included articles. In addition to rodents, ten studies using cats (Schweid et al., 2008; Bolzoni et al., 2013; Valdés-Cruz et al., 2019; Zhao et al., 2020; Ding et al., 2021; Pan et al., 2021), ferrets (Fröhlich and McCormick, 2010; D'Andola et al., 2018, 2019), or monkeys (Krause et al., 2017) were included. Among these included 213 papers, most studies applied tDCS *in vivo* to disease animal models (107 papers) or naïve animals (75 papers), while only 34 studies conducted *in vitro* experiments. Three papers included both *in vivo* and *in vitro* studies. We used (t)DCS in this manuscript to address *in vitro* studies with brain tissue.

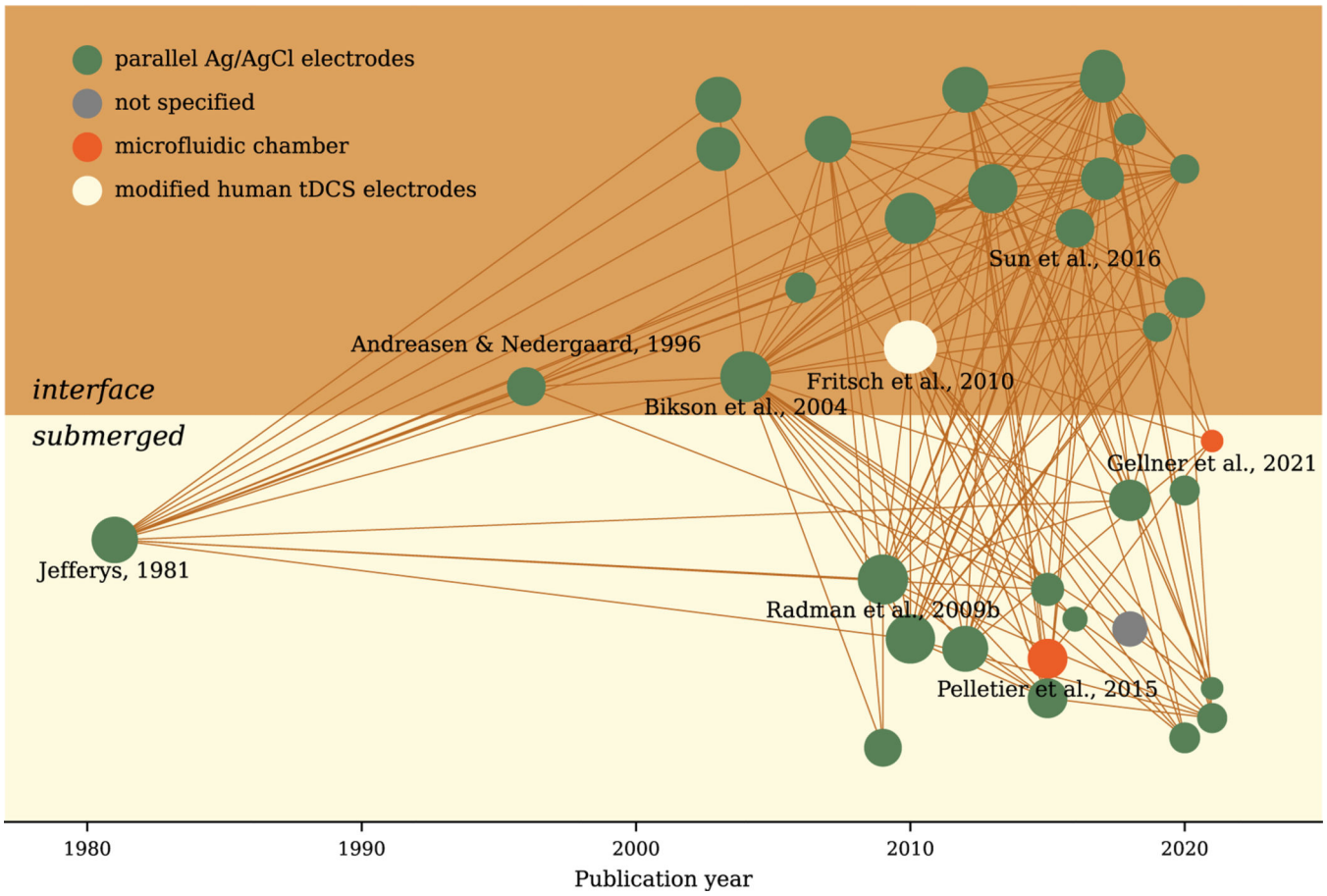

Fig. 2.

Literature bubble map of *in vitro* (t)DCS studies. Each dot represents one of the 34 selected and chronologically sorted. Dots in the upper panel (dark yellow background) indicate studies that used conventional interface chambers. Dots displayed in the lower panel (light yellow background) are studies that used conventional submerged chambers. A line is drawn between two dots if the later published one cited the former one. The dot sizes are proportional to the total counts of citations in the network. The dot colors indicate the method used to generate electric fields. Python package Kirsche (Ma, 2021) and citation data from Semantic Scholar were used to plot the map.

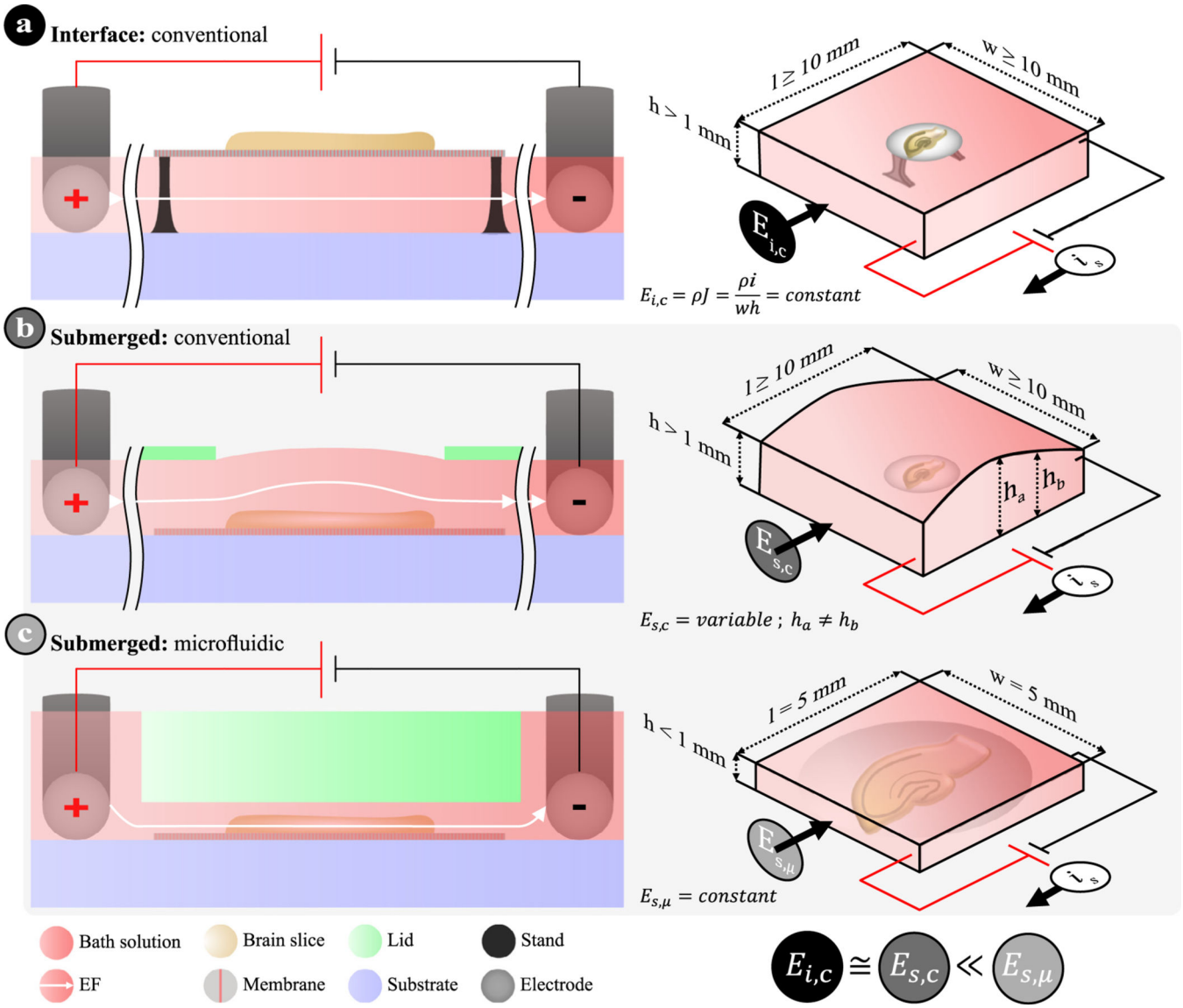

Fig. 3.

Schematics of different devices used in (t)DCS studies. (a) Conventional interface chamber where the organotypic brain slice on a porous membrane is supported by a stand with the bath solution below. (b) Conventional submerged chamber where the brain slice on a porous membrane is engulfed in bath solution (> 1 mm) and sitting on the substrate. In both (a) and (b), the open chamber design allows for the access of recording electrodes and/or immersed imaging objectives, where the evaporation of bath solution must be carefully monitored and controlled. Parallel Ag/AgCl electrodes are placed on either side to induce an EF. (c) Microfluidic chamber design, leveraged from electrotaxis experiments, where the brain slice on a porous membrane is submerged in a shallow and narrow fluidic microchannel while stimulation electrodes are placed in two reservoirs. The EF distribution (E) is either constant or variable depending on the cross-sectional area ($A = W \times h$) of the electrolyte body for any given input current density $\left(J = \frac{i_S}{A}\right)$ and electrolyte resistivity (ρ). The length (l) between

electrodes does not influence the EF intensity, but does directly impact the potential that is needed.

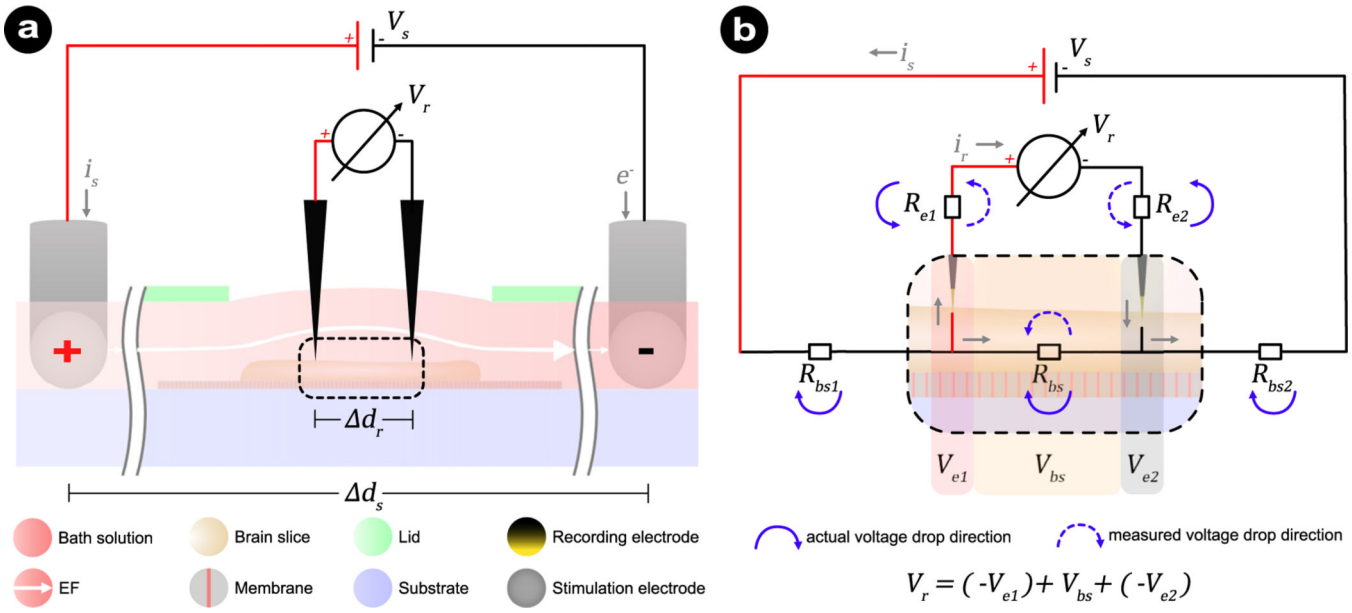

Fig. 4.

Schematics of calibration method and its equivalent circuit for measuring EF intensity in a submerged brain slice placed in an open chamber. (a) Two recording electrodes with a distance (Δd_r) apart are positioned along the electric field to record the voltage difference (V_r) and to approximate the EF intensity. (b) An equivalent circuit to dissect the components that contribute to the measured voltage (ΔV_r) from the voltmeter. The major contributions are from the brain slice (V_{bs}) and two recording electrodes (V_{e1} and V_{e2}). In the case of (t)DCS where only DC is applied, the capacitive characteristics of metal electrodes in electrolyte are equivalent to an open circuit and can be neglected. Therefore, a simplified equivalent circuit for the DC regime is highlighted here. Per definition, the unit of EF is volt per meter (V m^{-1}) or millivolt per millimeter (mV mm^{-1}), with the former being frequently used in human tDCS studies and the latter being more commonly used together with microfluidic applications. We decided to follow the convention of microfluidic studies and use the unit mV mm^{-1} throughout the manuscript.

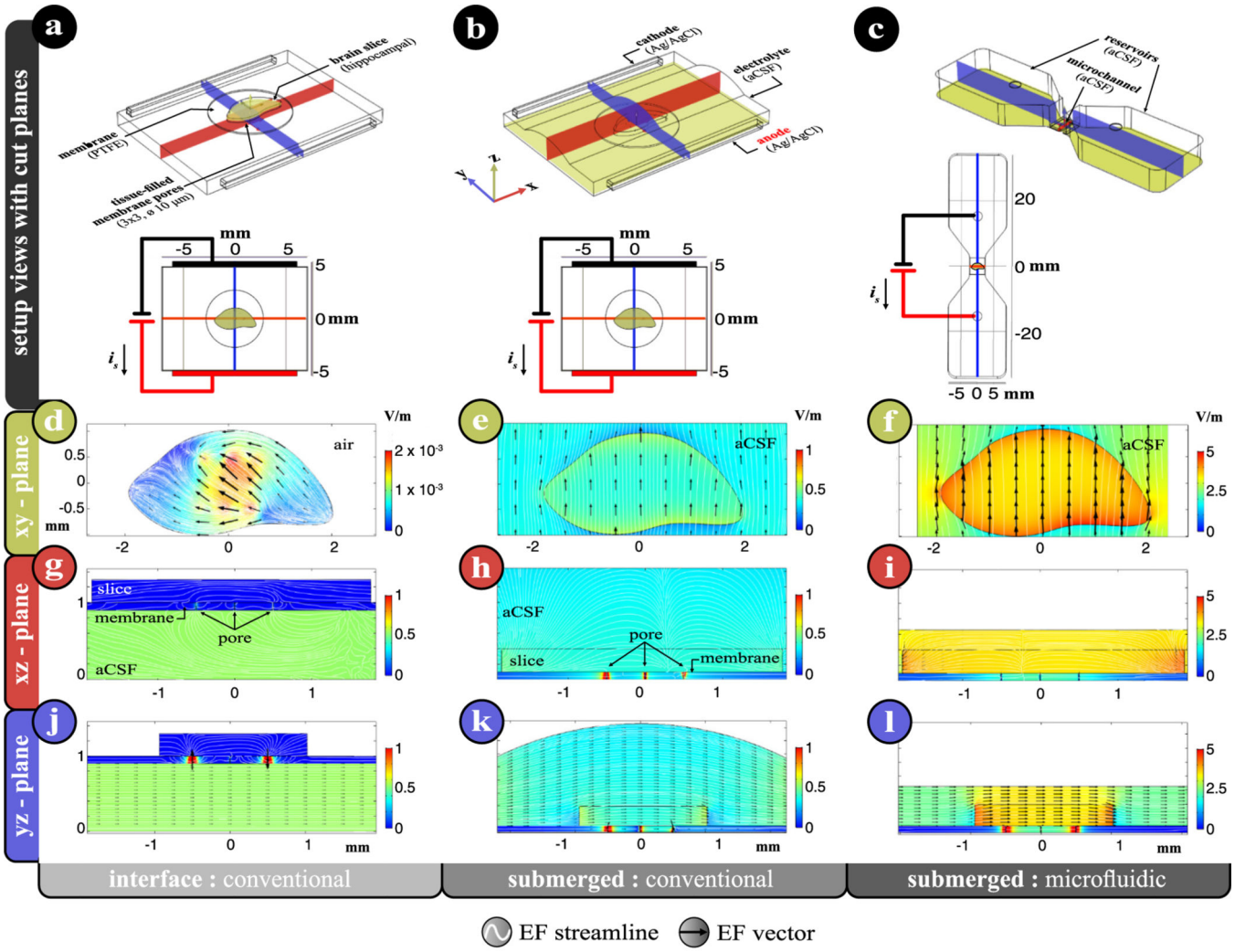

Fig. 5.

FEA simulation of EF distribution in different chamber designs. (a–c) Three-dimensional global view (first row displays the isometric view and second row is the top view) showing the geometric setup of conventional interface chamber, conventional submerged chamber, and microfluidic chamber designs. Positive stimulation current (i_s) flows from anode (in red) to cathode (in black). For (b), a meniscus over the tissue is analogous to the setup seen in Figs. 3 and 4, where it is open to atmosphere for *in situ* EF calibration. For all cases, the same input current (i_s = 10 μA) and same electrode–electrolyte contact area (6 mm^2) is used. (d–f) The *xy*-plane (in yellow) is the mid-plane (h = 0.15 mm) of the brain slice for all cases. Black arrows show the EF vector (i.e., direction and relative magnitude), while the white lines show the normalized streamlines. (g–i) EF distribution of mid-plane parallel to the stimulation electrodes (*xy*-plane). (j–l) EF distribution of the mid-plane perpendicular to the stimulation electrodes (*yz*-plane). The EF-range varies greatly case-by-case. Therefore, to highlight the EF distribution within the brain slice, the EF scale is not the same for all cases.

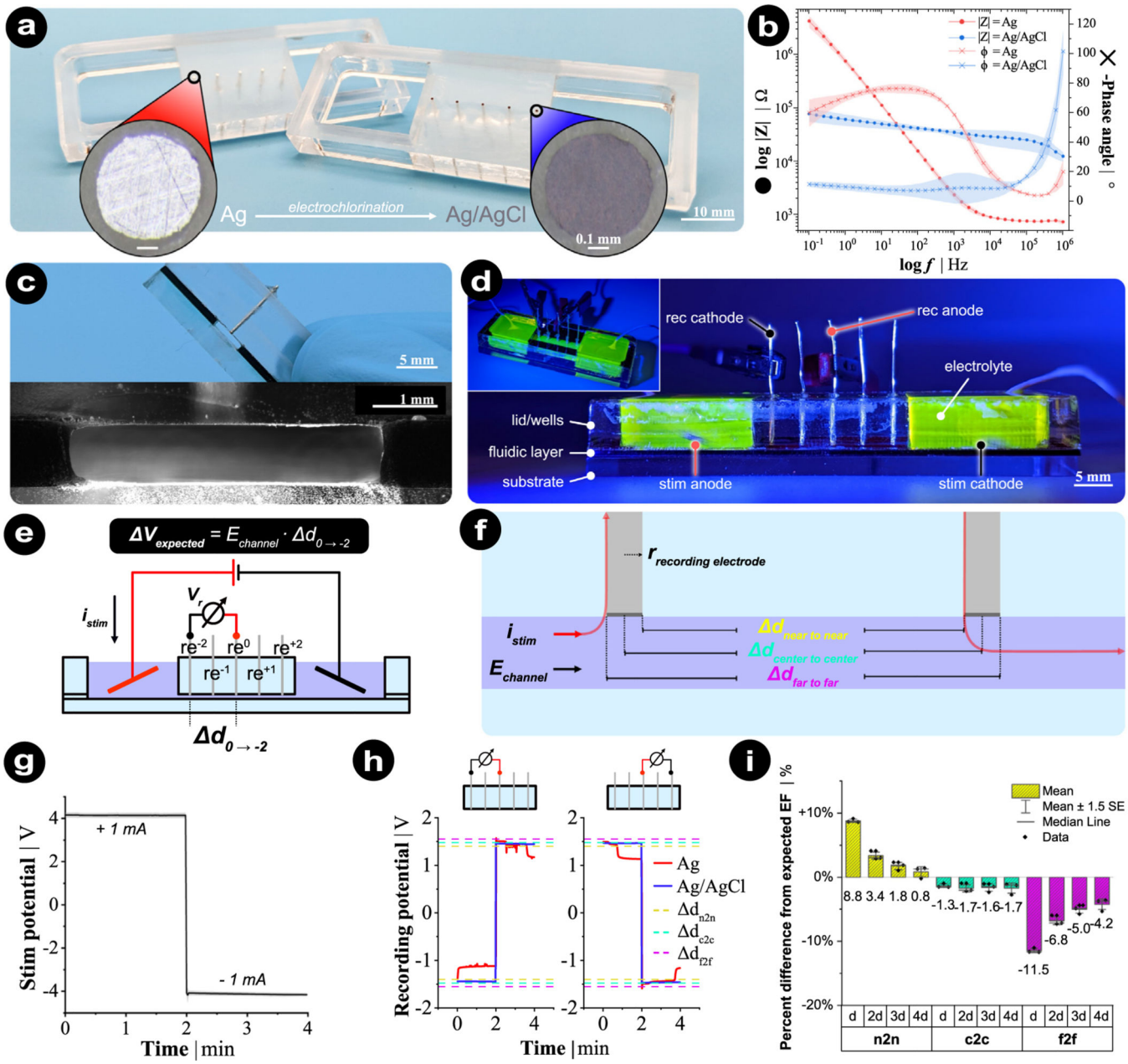

Fig. 6.

Measurement of EF with Ag/AgCl electrodes within the rectangular microchannel of a microfluidic chamber. (a) Bottom-side view of an acrylic lid with fixated recording electrodes that were sanded flush to the acrylic surface. Both Ag (left lid, red) and AgCl (right lid, blue) were tested. (b) Electrochemical impedance spectroscopy characterizing the impedance and phase difference of Ag (red) and AgCl (blue) recording electrodes. (c–d) Cross-section and side view of fully-assembled device with stimulation and recording electrodes. 10 mM PBS was used for all measurements. Fluorescein was used to visualize the fluidic architecture. (e) Expected voltage (V_{expected}) is calculated respectively for any given recording gap (Δd). (f) Three definitions of electrode gap distance. Two adjacent

recording electrodes have a c2c distance of 5.0 mm, while the n2n and f2f distances are 4.5 and 5.5 mm, respectively since the electrode radius is 0.25 mm. The red line shows the flow of the stimulation current through the recording electrodes when the current flows from right to left. (g) Stimulation protocol for all experiments (n = 12). The shaded area depicts the standard deviation. (h) Example recorded traces for 2 different configurations. Dashed reference lines are the expected voltage values by gap definition. (i) Percent difference from expected EF for different gap definitions.

Table 1

in vitro animal studies in (t)DCS.

Publication	System	Chamber type	Bath solution	Generating EF	Calibrating EF
Jefferys (1981)	rodent hippocampal slices[a]	submerged	aCSF	parallel electrodes	not specified
Andreasen and Nedergaard (1996)	rat hippocampal slices	interface	aCSF	parallel electrodes	measured by 2 electrodes
Bikson et al. (2003)	rat hippocampal slices	interface	aCSF	parallel electrodes	measured by 2 electrodes
Lian et al. (2003)	rat hippocampal slices	interface	aCSF	parallel electrodes	not specified
Bikson et al. (2004)	rat hippocampal slices	interface	aCSF	parallel electrodes	measured by 2 electrodes
Radman et al. (2006)	rat hippocampal slices	interface	aCSF	parallel electrodes	measured by 2 electrodes
Radman et al. (2007)	rat hippocampal slices	interface	aCSF	parallel electrodes	measured by 2 electrodes
Radman et al. (2009a)	rat M1 slices	submerged	aCSF	parallel electrodes	not specified
Radman et al. (2009b)	rat M1 slices	submerged	aCSF	parallel electrodes	measured by 2 electrodes
Fritsch et al. (2010)	mouse M1 slice	interface	aCSF	human electrodes	not specified
Fröhlich and McCormick (2010)	ferret visual cortical slice	interface	aCSF	parallel electrodes	measured voltage gradient
Reato et al. (2010)	rat hippocampal slices	submerged	aCSF	parallel electrodes	measured by 2 electrodes
Kabakov et al. (2012)	rat hippocampal slices	interface	aCSF	parallel electrodes	not specified
Ranieri et al. (2012)	rat M1 slices	submerged	aCSF	parallel electrodes	not specified
Rahman et al. (2013)	rat M1 slices	interface	aCSF	parallel electrodes	not specified
Pelletier et al. (2015)	mouse cell cultures	submerged	medium	microfluidic chamber	calculated[c]
Reato et al. (2015)	rat hippocampal slices	submerged	aCSF	parallel electrodes	measured by MUE[d]
Chang et al. (2015)	mouse MT-ACC slices	submerged	aCSF	parallel electrodes	measured by MEA
Sun et al. (2016)	mouse hippocampal slices[b]	interface	aCSF	parallel electrodes	not specified
Lu et al. (2016)	mouse MT-ACC slices	submerged	aCSF	parallel electrodes	measured by MEA
Lafon et al. (2017)	rat hippocampal slices	interface	aCSF	parallel electrodes	not specified
Rahman et al. (2017)	rat M1 slices	interface	aCSF	parallel electrodes	not specified
Kronberg et al. (2017)	rat hippocampal slices	interface	aCSF	parallel electrodes	measured by 2 electrodes
D'Andola et al. (2018)	ferret V1 and V2 slices	interface	aCSF	parallel electrodes	measured voltage gradient
Latchoumane et al. (2018)	mouse cell cultures	submerged	medium	not specified	not specified
Chakraborty et al. (2018)	mouse PFC slices	submerged	aCSF	parallel electrodes	not specified
D'Andola et al. (2019)	ferret forebrain slices	interface	aCSF	parallel electrodes	not specified

J Neurosci Methods. Author manuscript; available in PMC 2023 February 01.

Publication	System	Chamber type	Bath solution	Generating EF	Calibrating EF
Ross et al. (2020)	human cell cultures	submerged	medium	parallel electrodes	not specified
Kronberg et al. (2020)	rat hippocampal slices	interface	aCSF	parallel electrodes	measured by 2 electrodes
Sun et al. (2020)	mouse hippocampal slices[b]	submerged	aCSF	parallel electrodes	not specified
Esmaeilpour et al. (2020)	rat hippocampal slices	interface	aCSF	parallel electrodes	measured by 2 electrodes
Farahani et al. (2021)	rat hippocampal slices	submerged	aCSF	parallel electrodes	measured by 2 electrodes
Gellner et al. (2021)	mouse cell cultures	submerged	medium	microfluidic chamber	calculated
Vasu and Kaphzan (2021)	mouse PFC slices	submerged	aCSF	parallel electrodes	not specified

[a] Guinea pig hippocampal slices; Jefferys (1981) and Andreasen and Nedergaard (1996) were included based on the citation history of the rest papers.

[b] Mouse hippocampal slices and human cortical slices.

[c] Calculated based on the conductivity of cell-free medium.

[d] Multiunit electrodes.

Table 2

Theoretical percent error of different recording systems.

Variable	$R_{V_r}(\Omega)$	$R_{e1}+R_{e2}(\Omega)$	$R_{bs}(\Omega)$	err_1	err_2	err_{total}
Tissue/channel resistance R_{bs}	10^7	10^5	10^2	−0.001%	−0.990%	−0.991%
Tissue/channel resistance R_{bs}	10^7	10^5	10^5	−0.980%	−0.990%	−0.991%
Tissue/channel resistance R_{bs}	10^7	10^5	10^8	−90.8%	−0.990%	−91.8%
Electrode resistance $R_{e1}+R_{e2}$	10^7	10^2	10^2	−0.001%	−0.001%	−0.002%
Electrode resistance $R_{e1}+R_{e2}$	10^7	10^5	102	−0.001%	−0.990%	−0.991%
Electrode resistance $R_{e1}+R_{e2}$	10^7	10^8	102	-10^{-4}%	−90.9%	−90.9%
Voltmeter resistance R_{V_r}	10^4	10^5	102	−0.091%	−90.9%	−91.0%
Voltmeter resistance R_{V_r}	10^7	10^5	102	−0.001%	−0.990%	−0.991%
Voltmeter resistance R_{V_r}	10^9	10^5	102	-10^{-6}%	−0.001%	−0.001%
n/a (this work)	10^7	1.4×10^5	7.4×10^2	−1.39%	−0.007%	−1.38%

The first error is due to too much current rerouted into the recording system. $err_1=\frac{R_{bs}}{R_{bs}+R_{e1}+R_{e2}+R_{V_r}}$.

The second error is due to significant voltage drop across the recording electrodes instead of voltmeter. $err_2=\frac{R_{e1}+R_{e2}}{(R_{e1}+R_{e2})R_{V_r}}$.

$err_{total}=err_1+err_2$.

Polarizable electrodes result in additional electrochemical reactions at the interface and is therefore excluded from this estimation.

Table 3

Material properties used in FEA.

Component	Width (mm)	Length (mm)	Height (mm)	σ (S m^{-1})	Relative permittivity
Brain slice	3.8	3.8	0.3	0.5 (Asan et al., 2019)	5×10^{7} (Asan et al., 2019)
PTFE membrane	5.0	5.0	0.1	1×10^{-16} (Nishi et al., 2012)	2 (Nishi et al., 2012)
aCSF	n/a	n/a	n/a	1.5 (Miceli et al., 2017)	80 (Miceli et al., 2017)
Ag/AgCl electrode	0.5	12.0	0.5	1.2×10^{-5} (Mebane and Maier, 2010; Pargar et al., 2018)	13 (Mebane and Maier, 2010; Pargar et al., 2018)
Conventional open chambers	14.0	10.0	1.0	-	-
Microfluidic chambers	5.0	5.0	0.7	-	-

The parameters are extracted from the cited publications.

Input conditions for FEA are $J = 1.67$ A m^{-2} for anode, 0 V for cathode, and 0 A for membrane.